Design and modelling of a passively powered Shoulder Elbow Perturbator

Author: Mauricio Saborío Ordóñez
Date: 28-FEB-2025

Design and modelling of a passively powered Shoulder Elbow Perturbator

By

Mauricio Saborío Ordóñez

In partial fulfilment of the requirements for the degree of:

Master of Science
in Biomedical Engineering
Track Medical Devices

at the Delft University of Technology,
to be defended publicly on Friday February 28, 2025 at 13:45

Supervisor:	Dr.ir. A.H.A. Stienen	
Thesis committee:	Prof.dr. H.E.J. Veeger,	TU Delft
	J.C. van Zanten	TU Delft

An electronic version of this thesis is available at http://repository.tudelft.nl/.

TU Delft

CONTENTS

***Abstract*—The Shoulder Elbow Perturbator (SEP) is a robotic diagnostic device developed to assess multiple forms of motor impairment common in stroke patients. As an active medical device, the SEP would be bound to strict regulations if brought to market. By replacing its motor with a passive power source, this regulatory burden can be minimized, with the added advantage of greatly minimizing its cost. As a first step in developing this passive SEP, a prototype capable of reproducing one of the SEP's basic tests was conceptualized. After evaluating multiple options for the passive energy source and associated components, a cost-effective design was developed using a spring, a variable radius winding drum to convert the spring's force output to a constant torque, and a bicycle disc brake. A simulation of this design was then modeled and run through a variety of scenarios as a theoretical validation of the concept. The results of this process are promising, though testing with a physical prototype is needed for further validation.**

I. Introduction

A. Stroke and its impact

A stroke refers to the disruption in the brain's blood flow either due to a blockage (ischemic stroke) or a hemorrhage (hemorrhagic stroke). It is a very common affliction, with an estimated prevalence of 101 million cases and incidence of 12.2 million cases per year worldwide [1]. Regardless of the cause, a stroke typically leads to localized damage to brain tissue. The effects of a stroke on the patient's health can vary based on factors such as its exact location and speed of treatment, but some form of upper limb motor impairment is frequently seen, presenting in 50-80% of cases [2]. This motor impairment typically as a combination of various aspects, with muscle weakness, spasticity, abnormal synergies, and loss of coordination or sensation being common [3].

B. Diagnostic methods

Over the years, several methods have been developed to evaluate the nature and degree of motor impairment in stroke patients, sometimes among other effects. The most widely used are assessments meant to be performed by physiotherapists and similarly trained professionals. Common assessment scales include:

- Fugl-Meyer Assessment (FMA) scale: Assesses factors such as reflex activity, movement coordination, and range of motion through a combination of patient-active tasks and patient-passive motions [4].
- Modified Ashworth Scale (MAS): Assesses spasticity by measuring the resistance or stiffness during patient-passive motions [5].
- Modified Tardieu Scale (MTS): Assesses velocity-dependent spasticity by measuring the magnitude of resistance or stiffness and the angle at which it occurs during patient-passive motions performed at different speeds [6].

Despite their widespread use, these methods have limitations. As all scoring is done by a human, there is a risk of both inter- and intra-evaluator variability. The scoring systems also range from 3- (FMA) to 6-point (MAS) scales, which reduces the specificity possible in results. These limitations can be compensated for by obtaining data, such as EMG activity, from various sensors, but this does not solve all issues. Just as scoring can be subject to variability, so can the test motions performed by an evaluator.

To ensure consistency between assessments, it has been proposed to replace the human performing the motions on the patient's body with an electronically controlled device [7]–[15]. Despite their advantages over traditional diagnostic methods, such devices have not seen widespread adoption. One reason for this may be their specificity. The exact presentation of post-stroke motor impairment varies per patient and, while a robotic device may excel at quantifying one aspect of it, it cannot provide a complete picture [16].

C. The Shoulder Elbow Perturbator

The Shoulder Elbow Perturbator (SEP), shown in Fig. 1, was developed to address this. [16]. It is provides a single solution for quantifying multiple motor impairments of these two joints common in stroke patients. As its name implies, mechanical perturbations are the primary tool it uses for this. These perturbations are powered by a high-torque, direct-drive servo motor (model TMS3C from HIWIN). It also incorporates a spring-based weight compensation mechanism. Combining these two, the SEP can apply perturbations to the elbow while providing varying amounts of support to the shoulder. To measure the patient's elbow reaction torque (ERT), the SEP uses a force sensor mounted between its main shaft and armrest.

For its initial development and validation, the SEP was used to perform a series of tests, each intended to quantify a different motor impairment [16], [17]. Together, these tests are referred to as the Re-Arm protocol [18]. These tests, and the parameters they measure, are:

- Maximum voluntary torque (MVT): The patient exerts as much elbow torque as they can while their arm is held at a 90° angle with full weight support.
- Abnormal synergy: With different amounts of weight support, the patient extends their elbow as far as they can.
- Spasticity: The SEP extends the relaxed patient's elbow at 100°/s with full weight support.
- Viscoelasticity: The SEP extends and then flexes the relaxed patient's elbow at 6°/s with full weight support.

In addition to these relatively simple tests, the SEP is capable of more complex operations. For instance, it has been used to apply perturbation following a multisine signal, with the resulting data being usable in system identification [18].

D. Medical Device Regulation

In its present state, the SEP is considered a research use only (RUO) device, and it is thus exempt from regulations that typically apply to medical devices [19]. If it were to be marketed, however, the SEP's use for diagnostic purposes would require it to adhere to various regulations specific to them. These regulations vary by region. All devices marketed within the European Union, for instance, must comply with what is commonly called the Medical Device Regulation (MDR) [20]. The MDR assigns all medical devices a classification based

Fig. 1. Photograph of the original SEP showing how the patient's arm is mounted. Adapted from [16].

on the potential risk to the patient using them, ranging from Class I (low risk) to Class III (high risk).

The MDR also makes a distinction between active and passive devices. Chapter I, Article 2 defines an "active device" as:

> "... any device, the operation of which depends on a source of energy other than that generated by the human body for that purpose, or by gravity, and which acts by changing the density of or converting that energy. Devices intended to transmit energy, substances or other elements between an active device and the patient, without any significant change, shall not be deemed to be active devices." [20, p. 16]

As the SEP's source of energy is electricity, which its motor converts to mechanical energy, it is classified as an active device. By replacing this motor with a mechanism powered by either a human or by gravity, however, it would be possible to create a similar device that would be considered passive. Such a device would have notable advantages when compared to an active one.

E. Advantages of a passive alternative

1) Regulatory requirements: The exact requirements for a medical device to be compliant with regulations depend primarily on its regulatory classification. Annex VIII, Chapter III, Rule 10 of the MDR states:

> "Active devices intended for diagnosis and monitoring are classified as class IIa:
> – if they are intended to supply energy which will be absorbed by the human body..." [20, p. 143]

As it applies mechanical energy to the body, the SEP would be classified as Class IIa at a minimum. A passive device with the same functions, however, would only be considered a non-invasive device which comes into contact solely with uninjured skin. This means that it, instead, falls under Annex VIII, Chapter III, Rule 1:

> "All non-invasive devices are classified as class I, unless one of the rules set out hereinafter applies." [20, p. 141]

There stringency of requirements for Class I devices is much lower than for Class IIa (or above) devices. One example of this that Class I devices require a post-market surveillance report, while Class IIa devices require a more comprehensive periodic safety update report [20]. Similarly, more requirements are laid out for documentation and validation as class increases.

Perhaps the most important factor in this gap is the involvement of notified bodies. Starting with class IIa devices, notified bodies become increasingly involved [20]. To ensure regulatory compliance for higher-risk devices, these bodies perform more thorough assessments, which increase development time and cost for devices. For class I devices, the conformity assessment procedure is instead carried out solely by the device's manufacturer themselves.

2) Cost: The model of the SEP's motor appears to be discontinued, making its original cost difficult to ascertain. However, those familiar with the SEP's development estimate it to be over €10,000. As will be addressed in subsequent sections of this report, the total cost of a passive version of the SEP would be a fraction of this component alone.

F. Goals

To evaluate the performance of a passive SEP (pSEP) against the original model, reproducing some of the latter's functions would provide a simple point of comparison. Given the early state of this research and the limited scope of this project, it would not be feasible to reproduce the SEP's full capabilities using a passive energy source. A more realistic goal would be to design a prototype which can perform simpler tests, such as those from the Re-Arm protocol.

Of these tests, only the spasticity and viscoelasticity tests would require engaging the pSEP's energy source, limiting the options to these two. In both tests, the perturbation follows a ramp and hold signal, but both present different challenges.

The spasticity test has a shorter time frame, meaning that a higher acceleration is required to have shorter ramp and longer hold durations. Additionally, the higher velocity elicits a larger ERT , which the pSEP would need a higher torque output to counteract [16]. With its slow velocity, the viscoelasticity test's main challenge is the use of perturbations in opposite directions. An additional mechanism to reverse the direction of torque from a single energy source, or a second energy source that engages after the first disengages, would likely be needed to accomplish this. As the spasticity test's challenges are more connected to the characteristics of the energy source itself, it was selected.

Therefore, the question which this project aims to answer is as follows:

> Is it possible to design a passive device which reproduces the SEP's capability to perform the spasticity test of the Re-Arm protocol?

Additionally, the pSEP should be able to generate ramp and hold perturbations following a variety of velocity profiles, such as a 6°/s one mimicking the extension phase of the Re-Arm protocol's viscoelasticity test.

II. Requirements, constraints, and performance criteria

Table I lists a summary of the requirements, constraints, and performance criteria set for this project. A detailed description of how each of these was defined can be found in Appendix A.

TABLE I
SUMMARY OF REQUIREMENTS, CONSTRAINTS, AND PERTFORMANCE CRITERIA

Category	Name	Description
Requirements	Passive power	Energy source does not match MDR definition of an active device.
	Velocity profile	Able to accelerate to target angular velocity, maintain this velocity, and decelerate back to a full stop.
	Required torque	Able to exert a minimum of 55 Nm throughout full perturbation.
	Range of motion	145° (-55° flexion to 90° extension). Able to function between any starting and ending angle within this range.
	Energy storage capacity	Able to store 140 J of potential energy.
	Safety	Protects user and patient from mechanisms. Prevents perturbation from exceeding range of motion.
Constraints	Frame width	Maximum 500 mm.
	Frame height	Maximum 490 mm.
Performance criteria	Velocity output metrics	Peak error, RSME, MAE, SSE, and settling time. Lower is better for all.
	Cost	Lower is better

III. Concepts

Most of the pSEP's components can be split into four main subsystems:

1) **Energy generation**: The passive energy source itself, which stores and releases mechanical energy.
2) **Energy transmission**: The components responsible for converting the energy released by the energy source into a usable form and transmitting it between subsystems.
3) **Energy application**: The components which directly transmit the mechanical energy to the patient during perturbations.
4) **Energy regulation**: The components responsible for counteracting the pSEP's torque output in order to control the net torque output.

Each of these subsystems has multiple possible options for implementation, requiring individual concept selection processes.

A. Energy generation

A passive energy source, in the context of this project, could also be called passive energy storage. When acted on by mechanical energy, a passive power source will store this energy before subsequently releasing it.

1) Falling weight: One option for an energy source is a falling weight, which, when lifted above a surface, stores gravitational potential energy. Calculations for this option are simple, as the force produced is constant, with the value calculated by the formula:

$$F_w = mg \tag{1}$$

where F_w is force output, m is mass, and g is gravitational acceleration.

2) Spring: A spring may also be used as an energy source, which stores elastic potential energy when deformed. Unlike a falling weight, the force output of a spring is not constant. Instead, for a linear extension spring, it increases according to the following formula:

$$F_s = F_{s0} + s_s k \tag{2}$$

where F_s is the spring's force output, F_{s0} is its preload (i.e., the force needed for the spring to begin deforming), s is its deformation, and k is its spring constant.

Assuming that the pSEP's torque output is proportional to the spring's force output, producing a desired torque requires a certain value of F, with any value below this being ineffective. Any deformation needed before reaching this value would, therefore, add to the space needed for the spring. Similarly, the fact that F continues to rise with deformation past this point also causes issues. The energy regulation mechanism used would need to be able to counteract the highest torque generated at the upper end of the deformation range used, meaning it would need to be stronger than one used with a constant force output.

3) Pneumatics: A pneumatic piston would, in practice, function similarly to a spring. As a passive device, a compressor could not be used to maintain a constant pressure throughout the piston's stroke. Therefore, like a spring, maintaining a usable force until the end of its stroke would require having a much higher force at the start of it.

4) Flywheel: A flywheel is notable for being a passive energy source option which directly outputs a torque, eliminating the need for linear force-torque conversion. However, it instead requires an additional mechanism to extract the stored energy, such as a clutch linking the flywheel to the main shaft. Storing enough energy for perturbations in a relatively small form factor could require accelerating the flywheel at a rate not possible for a human. In this case, a motor may need to be used, undoing some advantages of a passive device even if implemented in a way that prevents the device from being classified as active.

B. Energy transmission

1) Winding drum: The elbow's flexion/extension motion is a form of rotation, whereas most of the options considered for energy generation output linear force. To be usable for perturbations, this linear force must be converted to a torque. One simple solution for this would by the use of a standard winding drum, which outputs torque proportional to the force of its cable unwinding according to the formula:

$$T = Fr \tag{3}$$

where T is the torque output of the drum, F is the force pulling on the cable, and r is the drum's radius.

2) Variable radius drum: As an alternative to a standard, circular winding drum, it may be possible to design a winding drum whose radius changes over the course of a perturbation. The concept of such a variable radius drum (VRD) has been previously researched and validated, albeit with different implementations and purposes [21], [22]. In the pSEP, the VRD would be used to generate a constant torque output from a variable force input by balancing its radius with said input, as expressed by:

$$T = F_1 r_1 = F_2 r_2 = F_n r_n \tag{4}$$

where the subscripts indicate the values of F and r at any given point within the VRD's functional range.

3) Constant force mechanism: An alternative way to counteract the issues cause by the varying force output of energy sources, like springs and pneumatics, is to place these components in a constant force mechanism. By adding the energy source to a four bar linkage in a parallelogram arrangement, forces can be balanced in such a way that the force exerted at the endpoint of the linkage will be constant [23].

4) Clutch: Due to their fundamentally different structure compared to the other energy sources listed, flywheels require a unique mechanism to harness their stored mechanical energy. One solution for this is a clutch. A clutch is a mechanism that is used to connect and disconnect shafts in order to control the transmission of torque. A common application of clutches is in manual transmission cars, where the clutch could be considered to be normally closed. Disengaging the clutch stops the transmission from the engine's flywheel to the gearbox to allow for safe gear changes. This would be reversed in the pSEP, where a normally open clutch would engage to transmit torque from the flywheel to the shaft when higher torque is needed.

C. Energy application

This subsystem consists of the pSEP's armrest and its attached components. In the current SEP models, the armrest also incorporates a sensor which measures the torque generated by the patient's elbow. This overall concept will be retained for the pSEP, with adaptations made as necessary during the design process.

D. Energy regulation

Broadly speaking, the output of passive energy sources cannot be directly controlled in the same manner as that of a motor. In the absence of an external constraint, these sources will dissipate their stored potential energy at the maximum possible rate. Therefore, the pSEP must incorporate a subsystem which can regulate its output to achieve the desired velocity profile. This subsystem must be able to apply a negative torque high enough to fully counteract the pSEP's torque output and to decelerate the arm at the end of the perturbation. It must also be able to decrease this counter-torque to allow for acceleration both at the start of the perturbation and to correct when the patient's ERT causes the movement to go below the target velocity. The following concepts for energy regulation were considered.

1) Disc brake: A study on the use of bicycle disc brakes in rehabilitation exoskeletons demonstrated that their behavior was suitable for such applications [24]. By using a small motor to wind a cable attached to the bicycle brake's handle, it is possible to achieve a fine degree of control over the pressure applied to the brake disc by the brake pads and, therefore, the braking torque exerted.

2) Magnetorheological damper: A magnetorheological damper is a type of damper which takes advantage of the properties of a magnetorheological fluid [25]. These fluids change their viscosity in response to magnetic fields, allowing dynamic control of damping characteristics through the use of electromagnets. Rotary dampers, which would be the form used in the pSEP, have found medical usage in devices such as knee prosthetics [26].

IV. Concept Selection

For the concept selection process, combinations of the concepts for each subsystem were considered. Table II summarizes which options for the energy generation and transmission subsystems are compatible with each other. A "+" indicates that combination is compatible, "-" indicates that combination is wholly or partially incompatible.

Energy regulation was not included as both concepts should be compatible regardless of the selection made for the others.

A. Energy generation

As a first step in selecting an energy generation concept, calculations were performed to estimate the specifications needed for each one to fulfill the requirements.

For the falling weight, a Python code, seen in Appendix B was used to iterate through combinations of force (and, therefore, mass), winding drum radius, and fall distance to

TABLE II
COMPATIBILITY OF ENERGY GENERATION (LEFTMOST COLUMN) AND ENERGY TRANSMISSION CONCEPTS (TOPMOST ROW)

	Circular winding drum	VRD	Constant force mechanism	Clutch
Falling weight	+	-	-	-
Spring	-	+	+	-
Pneumatics	-	+	+	-
Flywheel	-	-	-	+

and find an optimal combination for fulfilling the torque and range of motion requirements. The selected combination had the following values:

- Force/mass: 323.53 N / 32.98 kg
- Fall height: 0.43 m
- Radius: 0.17 m

As stated in the requirements, the pSEP must be able to store 140 J of energy in order to fulfill its torque and range of motion requirements. The gravitational potential energy of a falling weight can be calculated using the formula

$$U_w = F_g h \tag{5}$$

where U_w is potential energy, F_g is force due to gravity, and h is the fall height. Plugging in the relevant values:

$$U_w = (323.53\text{N})(0.43\text{m})$$
$$U_w = 138.39\text{J}$$

Which is approximately the expected value.

Similarly, the amount of deformation needed for a linear spring to store the same amount of elastic potential energy can be calculated with the formula:

$$U_s = \frac{ks_s^2}{2} \tag{6}$$
$$s_s = \sqrt{\frac{2U_s}{k}}$$

where U_s is elastic potential energy, k is the spring's spring constant and s_s is its maximum deformation. Based on the models available from a provider, a representative value of 1000 N/m was chosen for the calculation. Plugging in the relevant values:

$$s_s = \sqrt{\frac{(2)(140\text{J})}{1000\text{N/m}}}$$
$$s_s = 0.53\text{m}$$

While the exact value will change depending on the exact characteristics of the spring used, it can be estimated that around 0.5 m of deformation would be required.

Due to various challenges involved in using a pneumatic piston and a lack of clear advantages over a spring, the pneumatics concept was discarded at this point.

Unlike the previous options, a flywheel stores energy in the form of kinetic, rather than potential, energy. This stored energy is a function function of the flywheel's moment of inertia (MOI) and angular velocity:

$$E_f = \frac{1}{2} I_f \omega^2 \tag{7}$$
$$\omega = \sqrt{\frac{2E}{I_f}}$$

where E_f is the kinetic energy stored in the flywheel, I_f is the flywheel's MOI and ω is its angular velocity. To calculate the ω required, the MOI is needed first. While there are more efficent form factors, it is assumed that the flywheel would be a solid disc due to manufacturing limitations. Therefore, its MOI can be calculated using the formula:

$$I_f = \frac{mr^2}{2} \tag{8}$$

where m is mass and r is radius. This formula ignores the presence of the shaft which the flywheel would be mounted on, but, due to said shaft's much smaller radius relative to the flywheel's, its impact on the total MOI would be minor enough to be omitted for preliminary calculations.

Based on the size constraints of the pSEP, a flywheel radius of 20 cm was used for calculations. Assuming a thickness of 1 cm, its mass would be roughly 10 kg. This would make the flywheel's MOI:

$$I_f = \frac{(10\text{kg})(0.2\text{m})^2}{2}$$
$$I_f = 0.2\text{kgm}^2$$

Plugging the relevant values into Equation 7:

$$\omega = \sqrt{\frac{(2)(140\text{J})}{0.2\text{kgm}^2}}$$
$$\omega = 37.4\text{rad/s}$$

Therefore, the flywheel would need to be spun up to 37.4 rad/s. For reference, this is equivalent to 357.1 rpm.

1) Energy generation concept selection: With estimated specifications for each concept, each could be considered in terms of cost, size, and overall complexity. Table III shows a ranking of the energy generation concepts, with 1 being best.

TABLE III
RANKING OF ENERGY GENERATION CONCEPTS

	Cost	Dimensions	Complexity
Falling weight	2	3	1
Spring	1	2	2
Flywheel	3	1	3

The falling weight's main advantage is its simplicity. It only requires a circular winding drum to generate torque, which would likely be relatively simple to manufacture even if the desired diameter is not found among commercial products. Another advantage is that, if a form of weight such as pellets were used, fine-tuning the output at a later point would be simple. The flip-side of this is its inflexibility. A falling weight can only releases energy based on its vertical motion. Given the constrained height of the pSEP, this causes issues. In terms of cost, the most cost-effective option would likely be lead whose recent cost per kilogram, as of this writing, is around €2/32.kg. [27]. If it were possible to purchase the previously calculated 32.98 kg at this price, it would amount to €65.96.

Springs are much less costly by comparison, with extension springs from Tevema rarely exceeding €20 [28]. A spring, while taking up a large amount of space due to its linear form factor and need for a large deformation, can function in any orientation. This allows it to make use of the pSEP's unconstrained length dimension, but may require additional mechanisms to redirect its force. A spring further adds complexity due to needing a transmission subsystem to achieve a constant torque.

A flywheel would probably be the most compact of all the options, as it relies on rotational, rather than linear, motion. If a horizontal flywheel was used and all necessary components can be made to fit within the pSEP's constrained height, its footprint may need to be only slightly larger than the flywheel's area. However,

The spring concept was ultimately chosen for its low cost, relatively low complexity, and the flexibility it affords in efficiently arranging components.

B. Energy transmission

As previously mentioned, using a spring with a simple winding drum would cause issues which can be mitigated by achieving a constant torque. Therefore, the options considered for the energy transmission subsystem were a VRD and a constant force mechanism. Due to the large amount of spring deformation needed to store the necessary energy and the travel distance needed to cover the full range of motion, a constant force mechanism would not be practical for use within the pSEP's size constraints. Therefore, the VRD was chosen.

C. Energy application

As previously mentioned, the energy application subsystem will be a reproduction of the SEP's with adjustments made as needed.

D. Energy regulation

Due primarily to the potential high cost and difficulty in acquiring the necessary components, a magnetorheological damper was deemed impractical. A disc brake was chosen.

V. Design

A design for a pSEP prototype was made using the selected concepts. Fig. 2 shows the full design, with the following subsections detailing its various components and their design processes.

A. Energy generation

1) Spring selection: First, the spring model was selected. The chosen spring, model T33360 from Tevema [29], stood out among those available primarily due to its remarkably large maximum deformation of over 500 mm. This would make it usable without needing additional mechanisms to multiply the travel distance. The spring's maximum length is also nearly three times its original one, allowing for a more efficient use of space. The spring is labeled A in Fig. 2.

B. Energy transmission

1) VRD profile calculation: The VRD's profile could then be calculated based on the characteristics of the spring. These calculations were performed in the software MATLAB (by MathWorks), and the code for them can be found in Appendix C.

First, a target torque was set at 55 Nm. Next, a matrix was created, dividing the spring's deformation into 100 steps of equal length. Next, the spring's force output was calculated using Equation 2 as a function of the deformation at each step. As an additional safety margin, this output was limited to roughly 95% of the spring's rated maximum.

Following Equation 3, the target torque was divided by this force output to obtain the radius required at each step.

As a drum rotates, the difference in an attached spring's deformation at two drum angles is equal to the arc length at the drum's surface between the same angles. With a circular winding drum, this arc length would be consistent for adjacent steps at any point in the rotation, but this is not the case for a VRD. As the radius increases, the surface's curvature flattens, meaning that a greater angular distance is needed to cover the same arc length. Since it is known that the arc length of each is equal to the difference between the deformation at adjacent steps, and the radius at each step is also known, it is possible to calculate the angle of the VRD at each step using the formula:

$$\theta_{VRD} = \frac{s_{arc}}{r} \tag{9}$$

where θ_{VRD} is angle, s_{arc} is arc length, and r is radius. With the angle and radius known for each step, it was possible to calculate Cartesian coordinates for each. The coordinates of the steps required to achieve a 145° range of motion were imported to the software AutoCAD (by Autodesk) as a series of points, which were then used to generate a spline. This spline, pictured as the cyan portion in Fig. 3, is used as the "active" section of the VRD's perimeter—that is, the section which the cable rolls off of during a perturbation.

2) Cable and fittings: As the spring's maximum force output, 715.6 N, was known at this point, it was possible to select a cable rated to withstand it. A 3 mm, 7x19 was chosen for its rated workload of 136 kg (equivalent to 1334.16 N), and because its construction would give it flexibility to allow for components with smaller bending radii to be used [30].

Alongside the cable, the fitting it would be anchored to and the pulleys used to redirect it as necessary were chosen. An M8 eye bolt was chosen as it is rated for a 100 kg (981 N) 45° load and a 70 kg (686.7 N) horizontal load [31]. To optimize the use of space, the spring would be mounted diagonally at an angle of around 22.7°, making this sufficient.

3) VRD construction: Knowing the profile of the VRD's main section, the shaft's diameter and connection method, and the diameter of the cable, the VRD could now be designed. Certain choices informed the design. First, while the design goal for this project does not necessarily call for it, it was decided to make the VRD symmetrical, potentially allowing the same design to be used for both right and left arms with little effort. Second, the complex shape of the VRD limited manufacturing options, with fused deposition modeling 3D

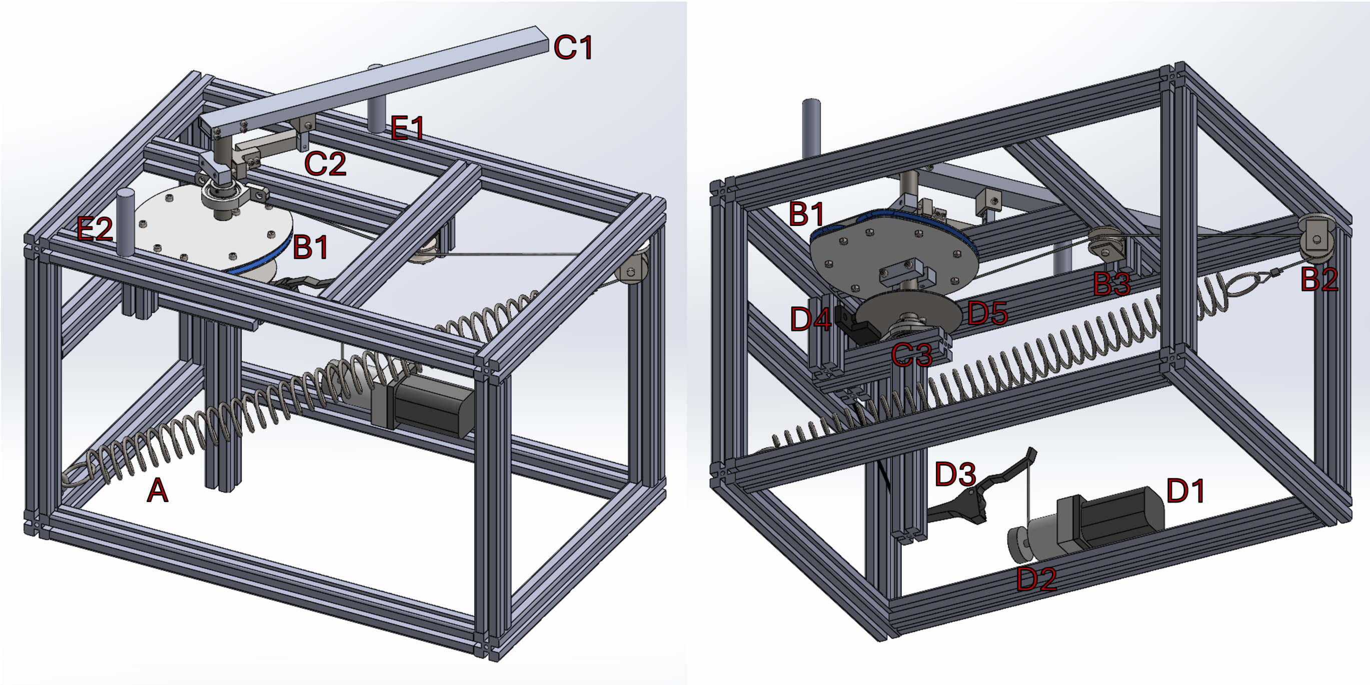

Fig. 2. 3D model of the pSEP prototype's final design. The labeled components are described in detail in Section V.

printing being chosen due to being most accessible and capable of making later adjustments to the design.

Due to the concerns related to the strength of 3D printed components, it was decided to manufacture the VRD in mutiple parts: a 3D printed core housing the groove for the cable and steel plate on either side of this core, all bolted together. As the steel plates and bolts would be responsible for most of the structure's, there was some freedom in regard to the core's design. This allowed a central channel to be incorporated into the core, with the cable being anchored to the main shaft rather than to the VRD itself, relieving stress on the weaker components. To lower bending stresses in the cable, sections with a radii of 30 mm, 10 times larger than the cable's diameter, were added between this channel and the active section of the VRD. Fig. 3 shows the profile of the VRD's core, while Fig. 4 shows the full drum assembly. Its position in the assembly is shown, labeled B1, in Fig. 2.

4) Shaft: The main shaft used in the pSEP must be able to withstand the high torques generated in it. Of the materials available from the university workshop, AISI 316 steel was chosen for its mechanical properties. The shear strength of this material is 400 Mpa [32]. By using this value and a known maximum torque, the minimum required diameter of a shaft can be calculated using the following formula [33].

$$D = 1.72(T_{max}/\tau_{max})^{1/3} \tag{10}$$

Where D is the diameter, T_{max} is the maximum torque, and τ_{max} is the shear strength. For a maximum torque of 50 Nm the equation becomes:

$$D = 1.72(50\text{Nm}/400 \times 10^6\text{Pa})^{1/3}$$

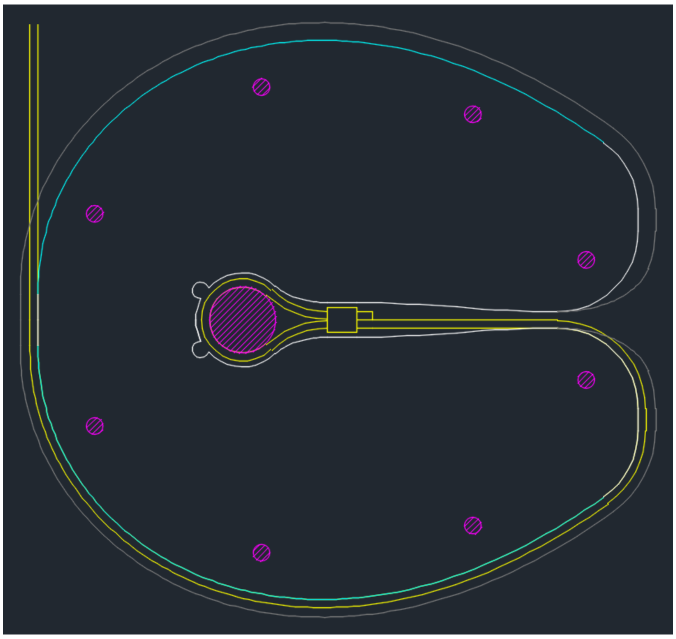

Fig. 3. The VRD core's profile. The sections colored cyan are those which the cable rolls off of during a perturbation. The outer lines colored gray represent the top of the cable groove. The areas with magenta hatching are the locations of the shaft and bolts. The cable, colored yellow, is positioned as it would be immediately prior to the start of a perturbation.

$$D = 8.6 \times 10^{-3}\text{m} = 8.6\text{mm}$$

For compatibility with components that would need to be purchased, such as bearings, it was chosen to use a 25 mm

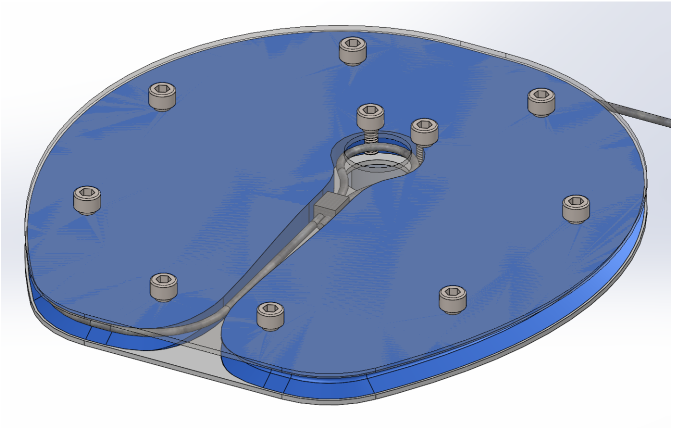

Fig. 4. A 3D model of the VRD. The upper steel plate has been made transparent to show the 3D printed core and the positioning of the cable.

diameter shaft of the same material, which also provides a comfortable margin of safety in the event that higher torques are generated.

It was also necessary to choose how the shaft and the components directly attached to it would be connected. Due to manufacturing limitations, the option chosen was to mill flat sections into the shaft, allowing clamps to be used to transmit torque between it and attached components. Fig. 5 illustrates this connection.

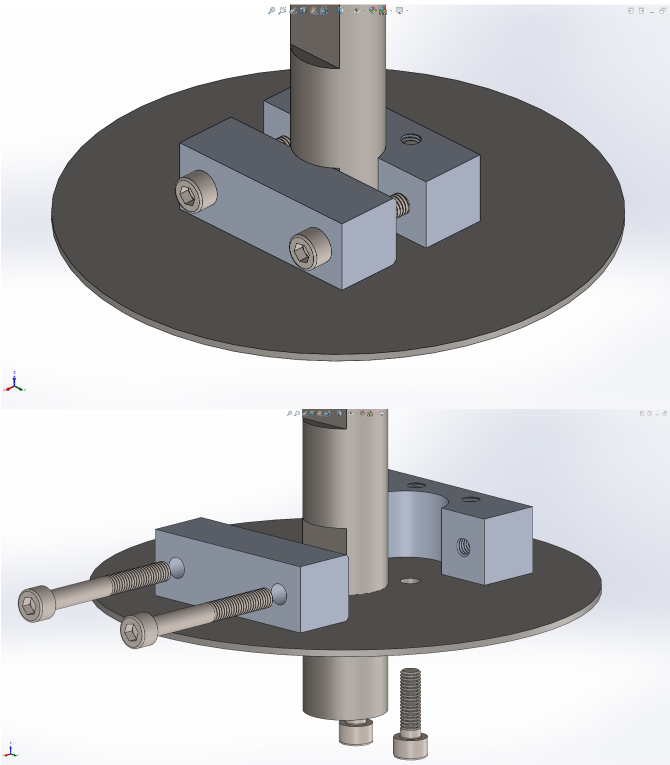

Fig. 5. Connection used to transmit torque between shaft and attached components. The upper image shows all components assembled. The lower image shows an exploded view of them.

C. Energy application

1) Armrest and sensors: The pSEP must, of course, have an armrest to which a patient's arm is secured during perturbations. This armrest must also be able to fulfill other functions, however. Firstly, the armrest has a key role in measuring the patient's ERT. By placing a sensor between the armrest and the shaft, it is possible to isolate the torques exerted on the former by the patient from those exerted by the other components on the latter. In order to do this, the armrest and shaft must be able to rotate independently of each other, allowing the torque difference to be focused on the sensor. One way to accomplish this is by connecting the two through ball bearings. A 40 x 20 mm aluminum pipe was selected as the material for the armrest. Two ball bearings are held in place inside the hollow pipe by several aluminum elements bolted to its walls. The end of the shaft, made thinner than the rest of it to provide a shoulder for the bearings to rest on, is inserted into the bearings through a hole in the bottom of the armrest. Spacers are used to prevent the bearings' inner rings and outer rings from touching the pipe's upper wall and the shaft's shoulder, respectively, preventing unwanted friction. Fig. 6 shows this setup while Fig. 2 shows its location when at maximum flexion, labeled C1.

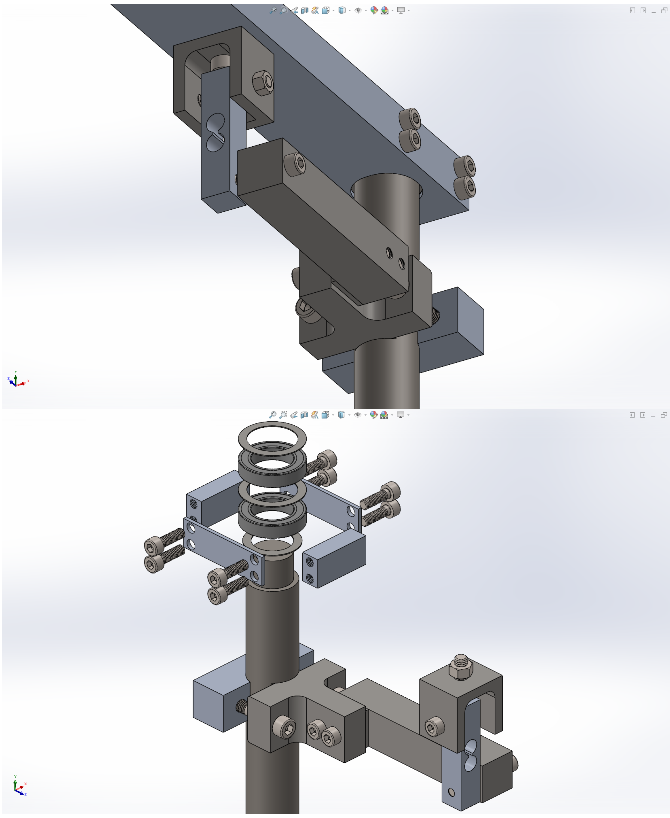

Fig. 6. The pSEP's shaft and armrest are connected through bearings to allow a degree of independent rotation. The upper image shows these components assembled. The lower image shows an exploded view of them with the armrest hidden. Both images also show the force sensor placed between the shaft and armrest.

Fig. 6 also includes the sensor mentioned above, while Fig.

2 shows it labeled C2. This is a single point load cell rated for a load of 50 kg (equivalent to 490.5 N) [34]. The load cell, intended to only be used in one direction, was oriented to measure ERT in the flexion direction and placed at a distance of 125 mm from the axis of rotation. Taking into account efficiency losses (detailed in the Modeling section below), the torque output of the pSEP would be roughly 52 Nm. By plugging these values into Equation 3, the maximum force possibly exerted on the load cell can be calculated:

$$F = 52\text{Nm}/0.125\text{m}$$
$$F = 416\text{N}$$

This is safely within the load cell's operating range. In the same way, the ERT can be calculated by multiplying the load cell's force reading and this known distance.

The armrest also has a role in loading the spring between trials. To do so, the operator must be able to apply a torque greater than than pSEP's in the opposite direction. As a solution to this, the armrest was simply made longer to act as a more effective moment arm. With a length of 500 mm from the axis of rotation, the force needed to move its endpoint can be calculated in the same way as was done above:

$$F = 52\text{Nm}/0.500\text{m}$$
$$F = 104\text{N}$$

This force is equivalent to that needed to lift 10.6 kg. Should this prove difficult for the operator, the armrest's hollow profile would allow for an object to be inserted and used to further extend the moment arm.

Along with ERT, the pSEP must also measure the angular displacement of the armrest, which it does through a magnetic encoder (AS5600) [35]. The encoder is placed directly below the shaft, labeled C3 in Fig. 2, with a small magnet attached to the center of the shaft's bottom face. Using an array of Hall sensors, the encoder can detect changes in the magnetic field as the shaft rotates.

D. Energy regulation

The setup used for this subsystem is an adaptation of the one designed developed in [24]. A motor (labeled D1 in Fig. 2) goes into a gearbox (D2), which rotates a small winding drum. This winding drum's cable is connected to the handle of a hydraulic bicycle brake (D3), pulling down on it as the drum rotates. This causes the brake caliper (D4) to close and apply pressure to the brake disc (D5), generating the braking torque. Fig. 7 shows these components isolated to provide a clearer image.

Notably, the brake used in the original study achieved braking torques of up to 120 Nm with a 0.7 Nm motor attached to a gearbox with a 1:20 ratio and a 0.12 m diameter disc. A larger disc had to be used to prevent interference between the brake caliper and the shaft clamp. This should result in a higher maximum braking torque, though the exact gain would need to be experimentally determined. The other notable change made from the original setup was simplification of the connection between the winding drum and the brake handle by removing a spring located between the two.

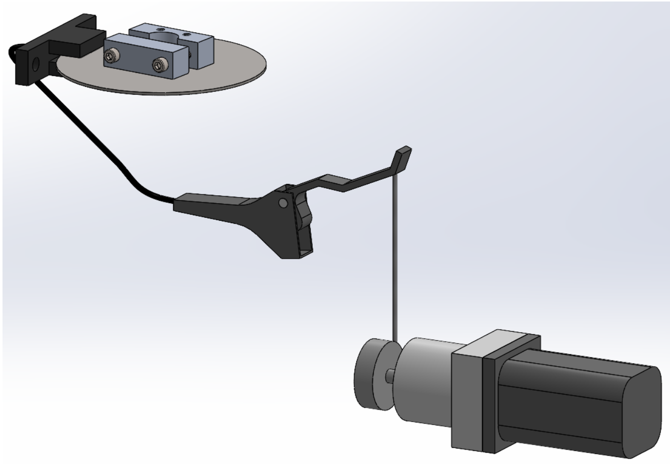

Fig. 7. The energy regulation subsystem isolated from all other components.

E. Other components

The following components of the pSEP do not fall under the four subsystems used so far in this report.

1) Frame: With the dimensions of the VRD and and spring known, the frame housing them could be designed. First, 40 x 40 mm aluminum extrusion profiles produced by item were selected as the material for their strength and compatibility with M8 bolts such as the one used by the eye bolt anchoring the spring. As stated in the Constraints section, the maximum width and height of the frame are 250 mm and 490 mm, respectively. Given the large amount of space required by the spring (769.1 mm at its longest extension), these values were used to minimize the frame length required.

2) Component arrangement: Prior to creating a 3D mock-up of the pSEP, a 2D model was used to determine the frame's required length and the appropriate placement of key components.

The VRD was placed, with the shaft at the midpoint of the frame's width, at one end of the frame. A pulley (B2 in Fig. 2) was placed at an opposite corner, where it would cause the VRD to extend the right arm of a patient as the cable unwinds. To optimize the use of space, the spring must be placed in line with opposite corners of the frame in both horizontal and vertical dimensions. The pulley was, therefore, aligned with said opposite corner, at which the eye bolt was placed. Taking into account the locations at which the spring and cable would connect to the eye bolt and pulley, an estimate for the available distance between the corners was made. The length of the frame was adjusted to 750 mm, making this estimated distance 816.8 mm, which was deemed enough to hold the spring at maximum extension along with the cable between it and the pulley, with a margin for error.

The cables coming off of the VRD at the start of the perturbation, when force is highest, and the pulley were extended until they intersected. At this intersection, a second pulley (B3 in Fig. 2) was added to redirect the path of the cable. The presence of this pulley in the cable's path affects the roll-off point (where the cable stops making contact with the VRD), which impacts the torque output. This discrepancy increases over the course of the perturbation, reaching around 4 mm at the end of it, which was deemed acceptable. Fig. 8 shows the 2D model, including elements illustrating some of the design process steps described above.

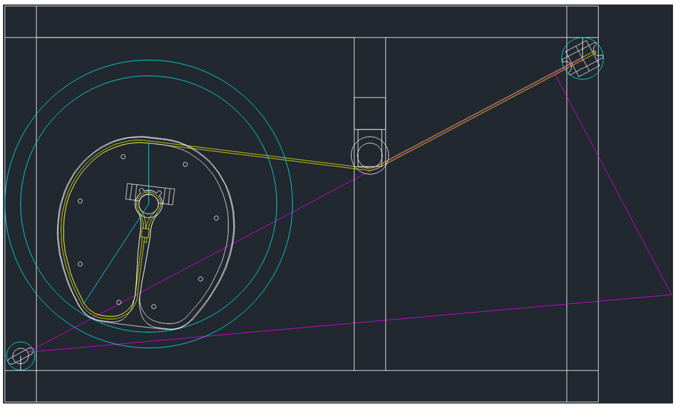

Fig. 8. A top view of the frame. The cyan circles around certain components represents an area which must be free of obstacles to rotate freely, with an additional clearance between the VRD and the outer wall of the frame. The elements in magenta represent an estimation of the length available for the spring. The right triangle's longer leg aligns with its position in the xy-plane, while the hypotenuse represents the length between the eye bolt and pulley's positions in 3D space.

3) Safety features: In order to fulfill the safety requirements set for the pSEP, various elements were added to the design:

- **Mechanical stops**: In order to prevent the pSEP from moving beyond its intended range of motion, mechanical stops were added. These are in the form of bars of round metal stock similar to that used for the pSEP's shaft. These bars reach halfway up the armrest's height to prevent pinching the patient's arm. At the end of each one is a section machined down and threaded with an M8 thread, which is screwed into nuts in the frame's slots. This allows the stops to be easily repositioned for tests using different ranges of motion. Fig. 2 shows these stops positioned to cover the pSEP's full range from maximum flexion (labeled E1) to maximum extension (E2).
- **Emergency stop**: A standard emergency stop button can be used to override the brake motor's control, forcing it to maximize the braking torque and stop the pSEP's motion.
- **Exterior paneling**: Though not shown in Fig. 2, all faces of the pSEP would be covered 1 mm-thick, removable, steel panels. These panels would prevent unplanned access to the pSEP's internal mechanisms and, should any component fail, block it from reaching anyone in the vicinity.

VI. Modeling

To perform a theoretical validation of the pSEP, a model of it was created in the software Simulink (by MathWorks) and tested under different conditions. Fig. 9 shows a simplified version of this model. The full model can be found in Appendix E, and the values used for the model's inputs are detailed in this section. The simulation can be split into the following phases:

1) **Start**: Initially, the armrest is at a predefined angle. The brake is fully engaged, resulting in zero net torque and velocity.
2) **Ramp up**: The braking torque is reduced, resulting in a positive net torque which accelerates the armrest.
3) **Stabilization**: As the motor's reaction is not instantaneous, the armrest's velocity overshoots the target hold value. The braking torque is alternately increased and decreased until a steady velocity is reached.
4) **Hold**: The armrest moves at a constant velocity for a given portion of the perturbation's range. To prevent acceleration, the net torque is maintained at zero by regulating the braking torque.
5) **Ramp down**: The braking torque is increased, resulting in a negative net torque which decelerates the armrest back to zero velocity.

The resulting velocity profile for a target hold velocity of 100°/s can be seen as the black line in the first plot in Fig. 10.

A. Energy generation

For any given armrest angle θ_{arm} in the pSEP's range of motion, a lookup table block is used to determine the spring's deformation based on interpolation of matrices generated by the code in Appendix C. The deformation is then multiplied by the spring constant and this product is added to the preload to find the spring's force output F_{spring}.

B. Energy transmission

The same lookup method is used to determine the VRD's radius at any θ_{arm}. The product of this radius and the spring's force output is multiplied by the pSEP's total efficiency to calculate the VRD's effective torque output T_{VRD}.

C. Energy application

The braking torque T_{brake}, discussed further below, and the ERT T_{elbow}, which is proportional to θ_{arm}, are subtracted from T_{VRD} to calculate the net torque at the armrest T_{net}. T_{net} is then divided by the system's total MOI to calculate the armrest's angular acceleration α_{arm}. α_{arm} is then integrated to calculate angular velocity ω_{arm}, which is again integrated to calculate θ_{arm}.

D. Energy regulation

A target velocity profile is calculated in a MATLAB function block as a piecewise function using values established in Appendix D. This block outputs a target angular velocity ω_{target} as a function of time. The difference between ω_{target} and ω_{arm} is the ω_{error}, which goes into a PID controller. The controller outputs a signal which is then limited to values between -1 and 1. A gain equal to the motor's maximum torque in Nm is applied to this limited signal. This then goes through a low-pass, second order Butterworth filter to represent the

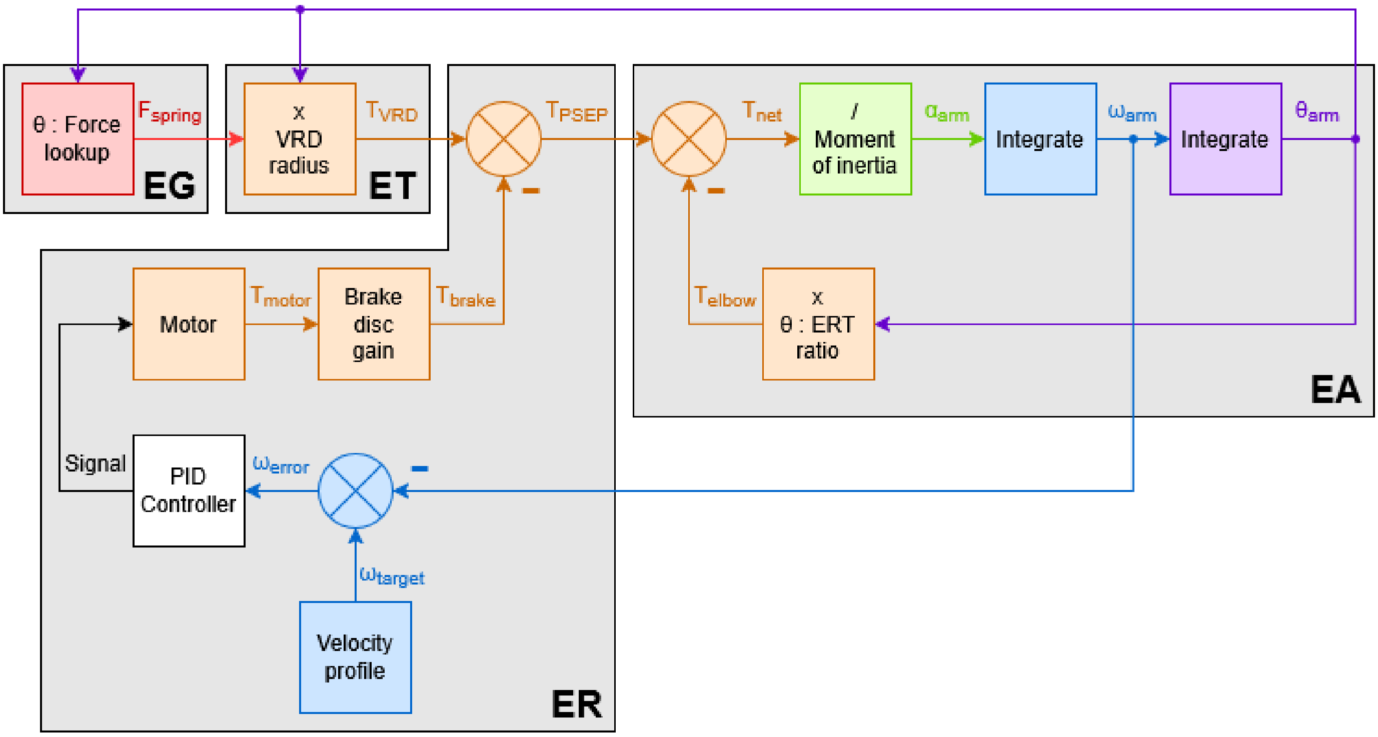

Fig. 9. Simplified Simulink model of the pSEP, with the subsystems divided into boxes labeled with their respective initials. The color of each block denotes its output: red is force, orange is torque, green is angular acceleration, blue is angular velocity, and purple is angle.

motor's response. The resulting output is the motor's torque T_{motor}. To approximate T_{brake}, a gain is applied to T_{motor}.

To better reflect a real use scenario, a sum block is used to add T_{VRD} to the brake output. This represents that the brake starts out fully countering the output torque to keep the armrest stationary prior to the perturbation.

E. *Initial conditions*

Initial conditions are primarily incorporated into the model using blocks to introduce values from the code in Appendix D.

1) Angle and range: The range of the perturbation was set to 90°, from -15° of flexion to 75° of extension. As the pSEP's range of motion begins at -55°, the initial angle is equivalent to 40°.

2) Velocity profile: Three target velocity profiles were created, each for one of the following target hold velocities: 100°/s, matching the Re-Arm protocol's spasticity test, 6°/s, matching the Re-Arm protocol's viscoelasticity test, and 150°/s, matching the highest velocity used in [13].

3) Efficiency: The pSEP's total efficiency was set at 94.13%. This was calculated as the product of the estimated efficiencies of all relevant components, such as pulleys and bearings.

4) Moment of inertia: The first elements contributing MOI are the rotating components of the pSEP itself, which can be divided into the shaft, including all its attached components, and the two individual pulleys. The MOI for these were estimated by isolating them in SolidWorks, placing a reference coordinate system at their respective axes of rotation, and extracting their mass properties. The total MOI of the device was set at 0.0485 kg*m^2.

The second element is the patient's forearm (and hand). The forearm was simplified to a uniform rod rotating about its end, allowing its MOI to be approximated using the following formula:

$$I_{arm} = \frac{m_{arm} L^2}{3} \tag{11}$$

where I_{arm} is the MOI, m_{arm} is the mass, and L is the length.

Elbow-grip length (measurement 31 in Fig. 11) and total body mass measurements from DINED were used here [36]. The mass of the forearm was then calculated based on ratios of body part mass relative to total body mass [37, Appendix II, Tab. A.2.3]. To represent extreme scenarios, calculations were done using both 5th percentile data for females and 95th percentile data for males:

$$I_{arm,f} = \frac{(1.05\text{kg})(0.294\text{m})^2}{3} = 0.0303\text{kgm}^2$$

$$I_{arm,m} = \frac{(2.6\text{kg}*)(0.395\text{m})^2}{3} = 0.1352\text{kgm}^2$$

Options for three scenarios were included in the model. In the first, only the pSEP's MOI is present. In the second and third, the weight of the smaller female forearm and larger male forearm, respectively, are added to this.

5) Elbow reaction torque: Four ERT scenarios were included in the model. In the first, there is no ERT. In the others, ERT is calculated as a function of angular displacement, ramping from zero at the start of the perturbation to a maximum value at the end of it. These maximum ERT values are: 10 Nm, close to the limit used in the Re-Arm protocol, 20 Nm, around the highest value seen in [13], and 50 Nm, an extreme scenario.

6) PID values: The values of the PID controller were manually tuned until a satisfactory output was achieved. During this process, it became apparent that the greatly reduced MOI in pSEP-only scenarios made it difficult for the velocity to stabilize. The following values were found to provide the best results when prioritizing performance in pSEP-only scenarios while remaining usable in pSEP and forearm scenarios:

- P: 0.0005
- I: 0.08
- D: 0.0004

However, a decision was made to prioritize the pSEP and forearm scenarios as these are more representative of the pSEP's intended use. As a result, velocity does not stabilize in pSEP-only scenarios when using the final values, which are:

- P: 0.001
- I: 0.1
- D: 0.001

7) Motor and brake: The motor's gain was set to 20, representing a maximum torque of 20 Nm. This value was chosen as representative of what could realistically be achieved using modern components in a setup similar to the one used in [24]. The Butterworth filter with a passband edge frequency of 2π*50 radians/s, representing an electrical bandwidth of 50 Hz.

The study on which the brake mechanism is based reported a maximum braking torque of 120 Nm using an input torque of 14 Nm [24]. This was approximated in the model by applying a gain of 9 to the motor torque to obtain the braking torque.

VII. Theoretical validation results

As stated in the performance criteria, the performance of the model in different scenarios was evaluated according to certain metrics. These were peak error, RMSE, MAE, SSE, and settling time. The MATLAB code used to calculate these can be found in Appendix F. Different velocity profiles result in different total durations, which would affect averages. To eliminate this issue, the range of values was restricted to the period between the beginning of the given profile's acceleration ramp and the end of its deceleration ramp. The values for the scenarios using the 100°/s target velocity profile are listed in Table IV. Similar results for all scenarios are included in Appendix G. Note that the SSE and settling time values were discarded for scenarios where no forearm MOI was present, as the calculations for these values require the velocity to stabilize. Fig. 10 shows output plots for velocity, armrest angle, and the torques present in the system for two scenarios using the 100°/s target velocity profile. To more clearly illustrate the influence of the parameters used, the results for the two most extreme stable scenarios were chosen for these plots.

VIII. Discussion

Table IV and Fig. 10 outline the different effects the different simulation scenarios have on the model's velocity output. By analyzing these different effects, it is possible to understand how different parameters impact the model's performance.

For instance, the difference between the red and blue lines clearly illustrates the impact of MOI. A higher MOI results in a larger overshoot and peak error, but reduces oscillations before stabilizing. It should be noted that, despite the different settling behaviors, a larger MOI only decreases settling time by 0.55% of the total perturbation time. Increasing ERT, on the other hand, has no impact on peak error or settling time, while noticeably affecting SSE and even decreasing the perturbation's range. Increasing either also has a smaller, but still present, impact on the various other error metrics used. By studying these impacts, it is possible to further optimize the pSEP's control system.

The simulation results suggest that a single set of controller values would not provide optimal performance across the full range of testing conditions the pSEP would be used under. This can be improved by tailoring these values to the parameters of each testing condition. For instance, an estimated MOI could be derived from physiological measurements, and a rough prediction of the ERT profile could be derived from an elbow MVT test. The pSEP's end users shouldn't be expected to manually tune the controller, so this would require a high degree of automation.

In addition to the output metrics, cost was set as a performance criterion. It is difficult to provide an accurate value as a full prototype was not built. Based on discussions with personnel familiar with the components used, a rough estimate for the total cost of the design is €2,000. The bulk of this, around €1,500, would be spent on the motor and its associated driver and gearbox. While future adjustments to the design may call for improved or additional components, the cost of a fully functional pSEP would likely be a fraction of the €10,000 that the SEP's motor alone is estimated to cost.

A. Limitations

Due to budgetary and time constraints, it was not possible to acquire and set up the motor for the energy regulation subsystem. This prevented building a full working prototype for testing, limiting the scope of the design's validation.

Due to the simple way in which ERT is calculated in the model, it is predictable and easy to adjust for. To more accurately model ERT may require a more refined approach, such as introducing velocity dependency and an element of randomness. Doing so could expose flaws in the control system that would need to be corrected.

The acceleration used in the Re-Arm protocol's original tests is not known. In order to accurately compare results obtained with the SEP and pSEP, the two should be made to match. This might cause issues if a high acceleration is required. While the pSEP's torque output is capable of accelerations much higher than those used in the simulation scenarios, a higher acceleration would lead to worse error

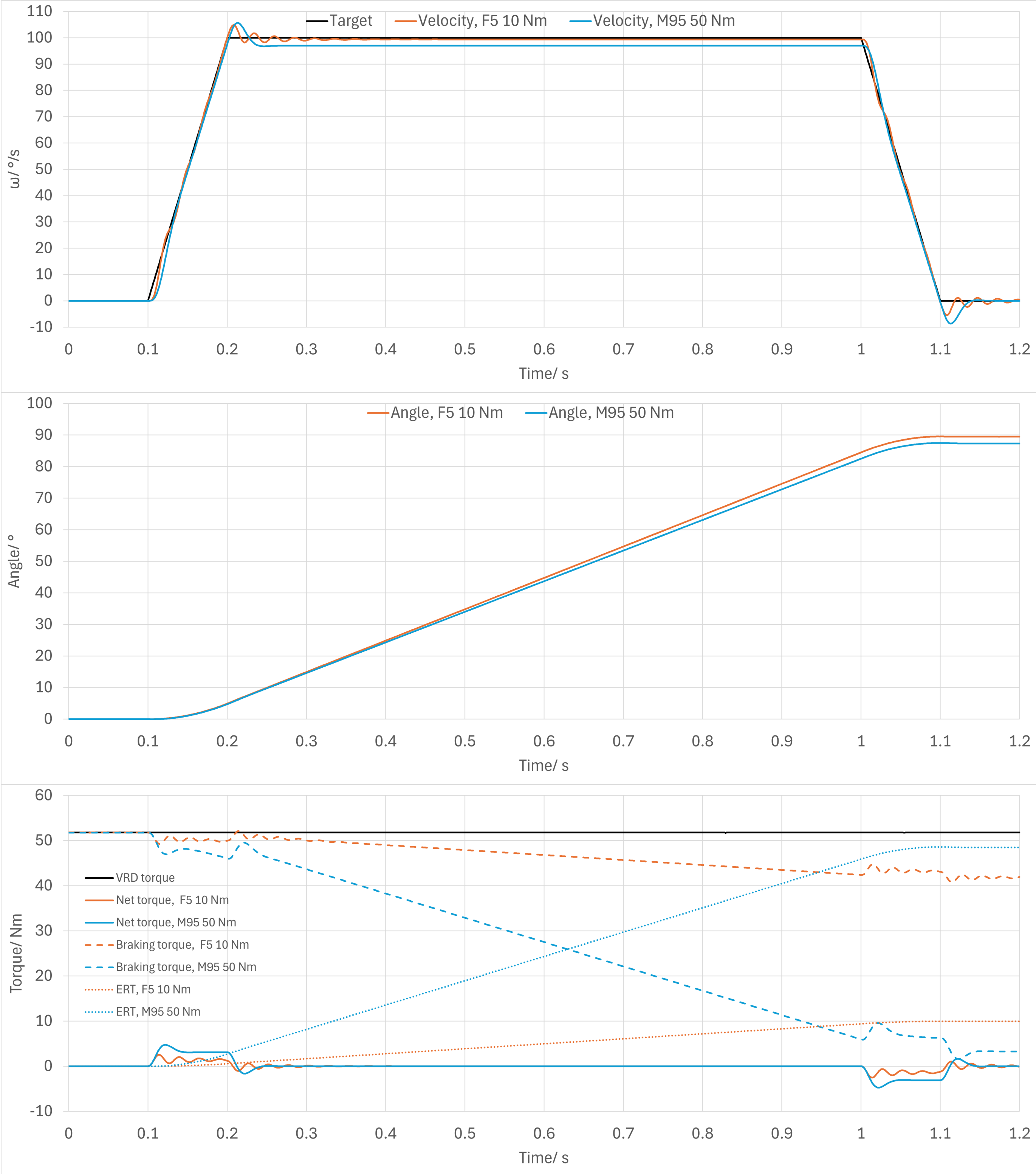

Fig. 10. Plots of various model outputs over time. In all plots, two scenarios are shown: a 5th percentile female arm MOI with ERT ramping to 10 Nm, in orange, and a 95th percentile male arm MOI with ERT ramping to 50 Nm, in blue. The first plot shows angular velocity outputs overlaid on the target velocity profile, in black. The second shows the armrest angle. The third shows various torques present in the system: the VRD's torque output in black, the net torque as solid lines, the braking torque as dashed lines, and the ERT as dotted lines.

TABLE IV
RESULTS FOR SCENARIOS USING THE 100°/S TARGET VELOCITY PROFILE

MOI sources	Max ERT/ Nm	Peak error		RMSE		MAE		SSE		Settling time	
		Value/ °/s	% of target hold velocity	Value/ °/s	% of target hold velocity	Value/ °/s	% of target hold velocity	Value/ °/s	% of target hold velocity	Value/ s	% of total time
pSEP	0	304.49	5074.76	202.80	3380.01	177.42	2956.94	N/A	N/A	N/A	N/A
	10	304.81	5080.17	190.24	3170.72	166.50	2775.04	N/A	N/A	N/A	N/A
	20	305.22	5086.97	172.30	2871.65	149.85	2497.42	N/A	N/A	N/A	N/A
	50	306.51	5108.52	125.56	2092.71	98.37	1639.44	N/A	N/A	N/A	N/A
pSEP + forearm (f)	0	0.35	5.80	0.02	0.27	0.00	0.03	0.00	0.00	0.24	1.55
	10	0.35	5.80	0.04	0.66	0.04	0.63	0.04	0.61	0.24	1.55
	20	0.35	5.80	0.07	1.24	0.07	1.22	0.07	1.22	0.24	1.55
	50	0.35	5.80	0.18	2.99	0.18	2.98	0.18	2.99	0.24	1.55
pSEP + forearm (m)	0	0.52	8.62	0.03	0.48	0.00	0.04	0.00	0.00	0.23	1.51
	10	0.52	8.62	0.05	0.76	0.04	0.64	0.04	0.61	0.23	1.51
	20	0.52	8.62	0.08	1.28	0.07	1.24	0.07	1.22	0.23	1.51
	50	0.52	8.62	0.18	3.00	0.18	2.99	0.18	2.99	0.23	1.51

metrics. A motor with a faster response time would mitigate this, but increase the pSEP's cost.

B. Future work

In order to make the pSEP a fully functional, and ideally marketable, device, much further work is needed. Limiting the scope to reproducing the Re-Arm protocol, the following recommendations for future steps can be given:

- Prototyping and validating: A physical, functional pSEP prototype must be built to compare its performance to the SEP when performing the Re-Arm protocol's spasticity test.
- Implementing dynamic control parameters: As discussed, a single set of control parameters, including PID values and target velocity, will not provide results of the same quality across all use scenarios. A protocol should be defined for determining the proper individualized values.
- Reducing dimensions: By including a mechanism that multiplies the spring's travel distance, it should be possible to use a shorter spring, reducing the pSEP's length. Due to the conservation of torque, this would likely require a spring with a higher force output, so care must be taken in ensuring that all components can withstand this.
- Making a design usable with either arm: The current pSEP design can only be used with a right arm. One solution to this could be to mount the pulley at the far end of the frame on a rail and place the spring's mounting point at the center of the frame rather than the corner. This would shorten the space available for the spring to deform and interfere with the vertical profile directly under the shaft, so the frame's design would need to be adjusted.
- Implementing other Re-Arm protocol tests: The current pSEP should already be able to perform the Re-Arm protocol's MVT test. The other two would require adjusting the design. A passive weight support system similar to the SEP's could be added to allow performing the abnormal synergy test. To perform the viscoelasticity test would require modifying the pSEP to allow it to reverse the direction of torque. This would effectively double the range of motion per perturbation and introduce other challenges which would be difficult to foresee at this point in time.

IX. CONCLUSIONS

The main goal of this project was to determine if it would be possible to design a passively powered device capable of reproducing the Re-Arm protocol's spasticity test. Within the scope of this project, the results indicate that the proposed pSEP design should be able to perform this function satisfactorily, though this cannot be conclusively stated without a full side-by-side comparison with the SEP for validation. The additional scenarios modeled also show that the pSEP has the versatility to be used for ramp and hold perturbations across a wide range of velocity profiles.

REFERENCES

[1] V. L. Feigin, M. Brainin, B. Norrving, S. Martins, R. L. Sacco, W. Hacke, M. Fisher, J. Pandian, and P. Lindsay, "World Stroke Organization (WSO): Global Stroke Fact Sheet 2022," vol. 17, no. 1, pp. 18–29, publisher: SAGE Publications. [Online]. Available: https://doi.org/10.1177/17474930211065917

[2] D. OâFlaherty and K. Ali, "Recommendations for upper limb motor recovery: An overview of the UK and european rehabilitation after stroke guidelines (2023)," vol. 12, no. 14, p. 1433. [Online]. Available: https://www.mdpi.com/2227-9032/12/14/1433

[3] L. A. Ingram, A. A. Butler, M. A. Brodie, S. R. Lord, and S. C. Gandevia, "Quantifying upper limb motor impairment in chronic stroke: a physiological profiling approach," vol. 131, no. 3, pp. 949–965. [Online]. Available: https://journals.physiology.org/doi/10.1152/japplphysiol.00078.2021

[4] A. R. Fugl-Meyer, L. JÃ€Ã€skÃ¶, I. Leyman, S. Olsson, and S. Steglind, "The post-stroke hemiplegic patient. 1. a method for evaluation of physical performance," vol. 7, no. 1, pp. 13–31.

[5] R. W. Bohannon and M. B. Smith, "Interrater reliability of a modified ashworth scale of muscle spasticity," vol. 67, no. 2, pp. 206–207. [Online]. Available: https://academic.oup.com/ptj/article/2728158/Interrater

[6] R. N. Boyd and H. K. Graham, "Objective measurement of clinical findings in the use of botulinum toxin type a for the management of children with cerebral palsy," vol. 6. [Online]. Available: https://onlinelibrary.wiley.com/doi/10.1111/j.1468-1331.1999.tb00031.x

[7] M. Mirbagheri, R. Harvey, and W. Rymer, “Mechanical properties of the elbow joint in spastic hemiparetic stroke subjects,” in *Proceedings of the Second Joint 24th Annual Conference and the Annual Fall Meeting of the Biomedical Engineering Society] [Engineering in Medicine and Biology*. IEEE, pp. 2449–2450 vol.3. [Online]. Available: https://ieeexplore.ieee.org/document/1053369/

[8] C. D. Takahashi and D. J. Reinkensmeyer, “Hemiparetic stroke impairs anticipatory control of arm movement,” vol. 149, no. 2, pp. 131–140. [Online]. Available: http://link.springer.com/10.1007/s00221-002-1340-1

[9] R. A. Scheidt and T. Stoeckmann, “Reach adaptation and final position control amid environmental uncertainty after stroke,” vol. 97, no. 4, pp. 2824–2836. [Online]. Available: https://www.physiology.org/doi/10.1152/jn.00870.2006

[10] R. D. Trumbower, V. J. Ravichandran, M. A. Krutky, and E. J. Perreault, “Altered multijoint reflex coordination is indicative of motor impairment level following stroke,” in *2008 30th Annual International Conference of the IEEE Engineering in Medicine and Biology Society*. IEEE, pp. 3558–3561. [Online]. Available: http://ieeexplore.ieee.org/document/4649974/

[11] C. G. Meskers, A. C. Schouten, J. H. De Groot, E. De Vlugt, B. J. Van Hilten, F. C. Van Der Helm, and H. J. Arendzen, “Muscle weakness and lack of reflex gain adaptation predominate during post-stroke posture control of the wrist,” vol. 6, no. 1, p. 29. [Online]. Available: https://jneuroengrehab.biomedcentral.com/articles/10.1186/1743-0003-6-29

[12] A. H. A. Stienen, J. G. McPherson, A. C. Schouten, and J. P. A. Dewald, “The ACT-4D: A novel rehabilitation robot for the quantification of upper limb motor impairments following brain injury,” in *2011 IEEE International Conference on Rehabilitation Robotics*. IEEE, pp. 1–6. [Online]. Available: http://ieeexplore.ieee.org/document/5975460/

[13] J. G. McPherson, A. H. A. Stienen, B. D. Schmit, and J. P. A. Dewald, “Biomechanical parameters of the elbow stretch reflex in chronic hemiparetic stroke,” vol. 237, no. 1, pp. 121–135. [Online]. Available: http://link.springer.com/10.1007/s00221-018-5389-x

[14] T. A. M. Plaisier, A. M. Acosta, and J. P. A. Dewald, “A method for quantification of stretch reflex excitability during ballistic reaching,” vol. 31, pp. 2698–2704. [Online]. Available: https://ieeexplore.ieee.org/document/10145802/

[15] K. Oh, W. Z. Rymer, and J. Choi, “A pilot study: effect of somatosensory loss on motor corrections in response to unknown loads in a reaching task by chronic stroke survivors,” vol. 14, no. 3, pp. 523–535. [Online]. Available: https://link.springer.com/10.1007/s13534-024-00348-5

[16] L. L. Van Der Velden, B. Onneweer, C. J. W. Haarman, J. L. Benner, M. E. Roebroeck, G. M. Ribbers, and R. W. Selles, “Development of a single device to quantify motor impairments of the elbow: proof of concept,” vol. 19, no. 1, p. 77. [Online]. Available: https://jneuroengrehab.biomedcentral.com/articles/10.1186/s12984-022-01050-2

[17] L. L. Van Der Velden, J. L. Benner, B. Onneweer, C. J. W. Haarman, R. Selles, G. Ribbers, and M. E. Roebroeck, “Reliability and validity of a new diagnostic device for quantifying hemiparetic arm impairments: An exploratory study,” vol. 54, p. jrm00283. [Online]. Available: https://medicaljournalssweden.se/jrm/article/view/12

[18] M. Van De Ruit, L. L. Van Der Velden, B. Onneweer, J. L. Benner, C. J. W. Haarman, G. M. Ribbers, and R. W. Selles, “System identification: a feasible, reliable and valid way to quantify upper limb motor impairments,” vol. 20, no. 1, p. 67. [Online]. Available: https://jneuroengrehab.biomedcentral.com/articles/10.1186/s12984-023-01192-x

[19] D.-G. f. H. a. F. S. . MDCG 2023-1 - guidance on the health institution exception under article 5(5) of regulation (EU) 2017/745 and regulation (EU) 2017/746 - january 2023 - european commission. [Online]. Available: https://health.ec.europa.eu/latest-updates/mdcg-2023-1-guidance-health-institution-exception-under-article-55-regulation-eu-2017745-and-2023-01-10_en

[20] “Regulation (EU) 2017/745 of the European Parliament and of the Council of 5 April 2017 on medical devices, amending Directive 2001/83/EC, Regulation (EC) No 178/2002 and Regulation (EC) No 1223/2009 and repealing Council Directives 90/385/EEC and 93/42/EEC,” 2017, official Journal of the European Union, L 117, 5 May 2017, pp. 1-175.

[21] J. Bieber, D. Bernstein, and M. Beitelschmidt, “Variable radius drum design for cable-driven parallel robots based on maximum load profile,” in *Cable-Driven Parallel Robots*, S. Caro, A. Pott, and T. Bruckmann, Eds. Springer Nature Switzerland, vol. 132, pp. 273–282, series Title: Mechanisms and Machine Science. [Online]. Available: https://link.springer.com/10.1007/978-3-031-32322-5_22

[22] L. Scalera, P. Gallina, S. Seriani, and A. Gasparetto, “Cable-based robotic crane (CBRC): Design and implementation of overhead traveling cranes based on variable radius drums,” vol. 34, no. 2, pp. 474–485. [Online]. Available: http://ieeexplore.ieee.org/document/8291529/

[23] R. H. Nathan, “A constant force generation mechanism,” vol. 107, no. 4, pp. 508–512. [Online]. Available: https://asmedigitalcollection.asme.org/mechanicaldesign/article/107/4/508/434440/A-Constant-Force-Generation-Mechanism

[24] A. H. A. Stienen, E. E. G. Hekman, A. C. Schouten, F. C. T. Van Der Helm, and H. Van Der Kooij, “Suitability of hydraulic disk brakes for passive actuation of upperâextremity rehabilitation exoskeleton,” vol. 6, no. 2, pp. 103–114. [Online]. Available: https://onlinelibrary.wiley.com/doi/10.1080/11762320902879888

[25] J. Carlson, D. Catanzarite, and K. St. Clair, “COMMERCIAL MAGNETO-RHEOLOGICAL FLUID DEVICES,” vol. 10, no. 23, pp. 2857–2865. [Online]. Available: https://www.worldscientific.com/doi/abs/10.1142/S0217979296001306

[26] H. Hsu, C. R. B. III, M. L. Palmer, R. J. Lukasiewicz, M. W. Lindsay, and S. W. Prince, “Magnetorheological fluid compositions and prosthetic knees utilizing same,” patentus 7 101 487B2. [Online]. Available: https://patents.google.com/patent/US7101487B2/en

[27] Daily metal price: Lead price (USD / kilogram) chart for the last 5 years. [Online]. Available: https://www.dailymetalprice.com/metalpricecharts.php?c=pb&u=kg&d=1200

[28] Extension springs tevema. [Online]. Available: https://webshop.tevema.com/gb/extension-springs/extension-springs

[29] T33360. [Online]. Available: https://webshop.tevema.com/gb/t33360

[30] staalkabel 7x19. [Online]. Available: https://www.rvspaleis.nl/kabel,-ketting,-toebeh./kabel-&-toebeh./7-x-19/m8036-4-3_1

[31] Product 65458008 - lifting eye bolt DIN 580 m8 x 13 steel c15e self coloured === user information at www.maedler.de in the section downloads ===. [Online]. Available: https://maedler.nl/Article/65458008

[32] ProtoXYZ | stainless steel 316. [Online]. Available: https://protoxyz.com/materials/metal/Stainless_Steel_316

[33] Shafts torsion. [Online]. Available: https://www.engineeringtoolbox.com/torsion-shafts-d_947.html

[34] Single point load cell - 50kg - 3135_0 - phidgets. [Online]. Available: https://www.phidgets.com/?prodid=226

[35] AS5600 magnetic angle sensor encoder module. [Online]. Available: https://www.tinytronics.nl/en/sensors/magnetic-field/as5600-magnetic-angle-sensor-encoder-module

[36] DINED. [Online]. Available: https://dined.io.tudelft.nl/en

[37] *Human Body Dynamics*. Springer-Verlag. [Online]. Available: http://link.springer.com/10.1007/b97432

[38] J. G. McPherson, A. H. Stienen, J. M. Drogos, and J. P. Dewald, “Modification of spastic stretch reflexes at the elbow by flexion synergy expression in individuals with chronic hemiparetic stroke,” vol. 99, no. 3, pp. 491–500. [Online]. Available: https://linkinghub.elsevier.com/retrieve/pii/S0003999317304859

[39] S. U. Islam, A. Glover, R. J. MacFarlane, N. Mehta, and M. Waseem, “The anatomy and biomechanics of the elbow.” [Online]. Available: https://openorthopaedicsjournal.com/VOLUME/14/PAGE/95/FULLTEXT/

Appendix A
Detailed Requirements, Constraints, and Performance Criteria

A. Requirements

To reproduce the spasticity test of the Re-Arm protocol using a passive energy source, the pSEP must fulfill several requirements.

1) Passive power: In order for the pSEP to be considered a passive device, it must not fall under the previously quoted definition of an active device. Therefore, the pSEP cannot incorporate a source of mechanical energy used for perturbations that is powered by anything other than a human body or by gravity. In all cases, this means that it must incorporate a passive mechanism to store energy. There are multiple options for loading this energy storage that would fulfill this requirement.

The first, and most simple, option is for the pSEP's energy storage to be a mechanism which can be manually loaded by a human. The second relies on interpretation of the second part of the MDR article, regarding energy transmission: a device is still deemed passive if it only transmits energy from an active device to the patient. Therefore, it would be possible to load the energy storage using an active device as long as this active device is not considered part of the pSEP.

2) Velocity profile: The pSEP must be able to generate a perturbation following a given velocity profile. This profile is composed of three stages:

1) Acceleration up to a target velocity.
2) Target velocity is maintained.
3) Deceleration from target velocity to a full stop.

For each of these stages, the pSEP must output a positive torque, zero torque, and negative torque, respectively. Throughout the perturbation, it must also be able to adjust torque to correct velocity changes due to ERT.

The main velocity profile used will have a hold velocity of 100°/s. However, being able to follow multiple profiles would be desirable, as it increases the pSEP's versatility.

3) Required torque: In order to reach and maintain a constant angular velocity, the pSEP must be able to, throughout the full length of a trial, exert enough torque to overcome any ERT generated in response to the motion. The motor used in existing SEP models exert a constant torque of 60 Nm, but it may not be necessary for the pSEP to match this. [16].

The pSEP's maximum torque output would also be directly proportional to its maximum angular acceleration per the formula:

$$\alpha = T/i \tag{12}$$

where α is angular acceleration, T is torque, and i is moment of inertia (MOI).

In the original experiments performed with the SEP, the device was programmed to stop the extension motion when ERT reached 11 Nm, so its actual maximum value is not known. [16], [17]. A similar experiment without such limits saw peaks close to 20 Nm, though these occurred at a higher angular velocity (150°/s). [13].

In addition to ERT, the torque requirement could, instead, be based on MVT. This would allow the same design to be used for a larger variety of tests. A study measured MVTs of up to 44.9 Nm in stroke patients [38]. Concurring with this, an expert on this topic recommended a value of 50 Nm.

As having a higher maximum torque would allow the pSEP to use a larger range of velocity ramp profiles in its perturbations, this higher value of 50 Nm was chosen. In order to account for losses due to efficiency and unforeseen factors, a value of 55 Nm was used as a target for calculations.

4) Range of motion: The human elbow's range of motion varies based on individual factors, but can be generalized as being 145° [39], from -55° of flexion to 90° of extension. Tests do not necessarily need to utilize this entire range. The pSEP should be able to cover the full range of motion and function regardless of the angles at which the perturbation begins and ends.

5) Energy storage capacity: With the requirements for torque and range of motion defined, it is possible to calculate the maximum amount of work which the pSEP would perform over the course of a perturbation. This is calculated using the formula:

$$W = T\theta_{total} \tag{13}$$

where W is the work, T is the torque, and θ_{total} is the total angular displacement. As θ_{total} must be in radians, a conversion factor is included in the calculation:

$$W = (55\text{Nm})(145)(\tfrac{\pi}{180}) = 139.19\text{J}$$

This work is equivalent to the amount of energy which the pSEP must be able to store in order to maintain this torque over the full range of motion. For convenience, the requirement will be rounded up to 140 J.

6) Safety: Patient and user safety should always be considered in a design process. In order to generate the torques needed, the stresses within the pSEP may reach dangerously high levels. In order to protect anyone near it both during normal operation and in case of failure, the pSEP must include safety features such as adequately strong external panels.

Additionally, it is necessary to ensure that the pSEP does not harm the patient. For instance, mechanical stops should be included to prevent exceeding the safe range of motion, and some form of emergency stop button must be implemented.

B. Constraints

For the pSEP to be at all usable, it must be possible for a sitting patient to position their elbow directly above its axis of rotation. Therefore, its maximum physical dimensions must be kept within ranges that prevent the interference between its frame and the patient's body. The two dimensions which must be constrained are the pSEP's width and height, discussed below. In order to determine this maximum distance, the 1-D Database of the DINED Anthropometric Database was referenced []. DINED's most recent dataset, from a 2004 study of Dutch adults aged 20-60, was used. Fig. 11 illustrates the relevant measurements from said study.

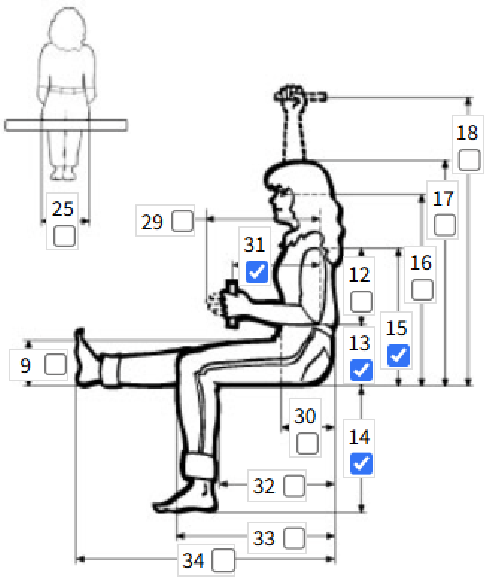

Fig. 11. Illustration showing measurements taken in DINED study [36].

1) Maximum width: The distance between the pSEP's side wall and axis of rotation cannot exceed the distance between a patient's torso and elbow. As shoulder-elbow length (measurement 12 in Fig. 11) was not taken in this study, the length was calculated as the difference between the sitting shoulder height (15) and elbow height (13). As the minimum length, excluding extreme cases, is the relevant value, the 5th percentile values were taken from the male and female groups included in the study. Table V shows these values.

TABLE V
DINED SHOULDER-ELBOW LENGTH VALUES

Measurement	Male	Female
Shoulder height, sitting/ mm	568	523
Elbow height, sitting/ mm	215	194
Shoulder-elbow length/ mm	353	**329**

The lowest value found, 326 mm, does not exactly reflect the distance between a person's torso and elbow due to the exact locations at which these measurements were taken. To account for this, a lower value, 250 mm, was chosen as the maximum distance between the device's wall and axis of rotation. For the pSEP to be usable with either arm, this would need to be true on either side of the axis, making the maximum width of the device 500 mm.

2) Maximum height: To accommodate patients of varied heights, who may sit on similarly varied chairs, the existing SEP models have an adjustable height. A passively powered pSEP should retain this feature. At the lowest height setting, it should be possible for the shortest patients to comfortably rest their elbow on the armrest during testing.

Assuming that the chair height is set to have the patient's feet resting on the ground, the maximum height for the armrest's surface can be calculated by adding the popliteal height (measurement 14 in Fig. 11) with the sitting shoulder height (15). These values for the fifth percentile of all groups in the study are included in Table V.

TABLE VI
DINED SITTING SHOULDER HEIGHT VALUES

Measurement	Male	Female
Shoulder height, sitting/ mm	568	523
Popliteal height, sitting/ mm	438	393
Total shoulder height, sitting/ mm	1006	**916**

As before, the lowest value must be adjusted due to the measurement location. Taking these factors into account, the maximum total height was set at 880 mm. Additionally, not all of the pSEP's height would be available to house the perturbation mechanism. Some of the current SEP models' heights are occupied by other components, such as a jack for height adjustment and a weight compensation mechanism for the arm. While the pSEP prototype will not incorporate these components, they are taken into consideration. Based on measurements taken from the SEP models, the maximum height of the prototype's frame should be 490 mm.

C. Performance criteria

1) Velocity output characteristics: To evaluate the performance of the pSEP, its output velocity can be logged and measured against a target velocity profile. The difference between these, or error, at given time points can also be logged. Based on these values, the following metrics can be found:

- **Peak error**: the maximum absolute error value reached.
- **Root mean square error (RMSE)**: the square root of the average squared error value, indicating overall deviation.
- **Mean absolute error (MAE)**: the average absolute error value, representing typical error magnitude.
- **Steady-state error (SSE)**: the error between the target hold velocity and the output velocity after stabilizing.
- **Settling time**: the time taken for the output velocity to stabilize. In this case, stability is considered to be reached when the velocity remains within 2% of the steady state value.

2) Cost: As previously noted, the total cost of the pSEP prototype would likely be a fraction of the SEP's motor alone. However, the pSEP's low cost is one of its key advantages, so this remains a criterion worth evaluating.

APPENDIX B
PYTHON CODE FOR OPTIMIZATION OF FALLING WEIGHT PARAMETERS

In [1]:

```python
import numpy as np
import csv

# Constants
t_arm = 55  # Nm
ratios = [1 / 5, 1 / 4, 1 / 3, 1 / 2, 1 / 1.5, 1, 1.5, 2, 3, 4, 5]
range_arm = 145 * np.pi / 180
radius_min = 0.03
radius_max = 0.2
radius_step = 0.01

# Function to calculate force
def calculate_force(t_arm, ratio, radius):
    t_source = t_arm / ratio
    force = t_source / radius
    return force

# Function to calculate distance
def calculate_distance(range_arm, ratio, radius):
    range_source = range_arm * ratio # radians
    rotations = range_source / (2 * np.pi)
    distance = rotations * (2 * np.pi * radius) # m
    return distance

# Initialize variables to store the optimal values
optimal_ratio = None
optimal_radius = None
min_force = float('inf')
results = []

# Iterate through possible values of ratio and radius
for ratio in ratios:
    radius = radius_min
    while radius <= radius_max:
        force = calculate_force(t_arm, ratio, radius)
        distance = calculate_distance(range_arm, ratio, radius)

        # Store the results of each iteration
        results.append((ratio, radius, force, distance))

        if distance <= 0.45 and force < min_force:
            min_force = force
            optimal_ratio = ratio
            optimal_radius = radius

        radius += radius_step

# Write results to CSV
with open('optimization_results.csv', mode='w', newline='') as file:
    writer = csv.writer(file)
    writer.writerow(["Ratio", "Radius (m)", "Force (N)", "Distance (m)"])
    writer.writerows(results)
```

In [ ]:

APPENDIX C
MATLAB CODE FOR VRD CALCULATION

```
% Inputs
    % Torque
        % Desired torque at arm
        torque_arm = 55; % Nm

    % Spring constant
        % Spring constant of a single spring
        k_base = 1.33; % N/mm
            % C (N/mm)

        % Number of springs in parallel
        parallel_amount = 1;

        % Number of springs in series
        series_amount = 1;

    % Length
        % Length of undeformed spring
        length_0 = 277; % mm
            % Lo

        % Maximum deformation
        deformation_1_max = 518.29 ; % mm

    % Force
        % Preload of spring
        preload = 61.11; % N
            % Fo

    % Ratios
        % Ratio of radii of pulleys in a speed reduction belt drive
        reduction_ratio = 1;

        % Ratio of radii of two connected, concentric pulleys
        concentric_ratio = 1;

    % Matrices
        % Number of rows matrices should initially have
        rows = 100;

        % Rows dropped from the start of matrix
        calc_start = 5;
            % As a safety margin to not reach plastic deformation
            % To reduce the maximum force

        % Rows dropped from end of matrix
        calc_end = 44;
            % To prevent more extreme shapes

% Calculations
    % Torque
        % Torque needed at the main drum
        torque_target = torque_arm / reduction_ratio ; % Nm

    % Spring constant
        % Total spring constant for springs in parallel
```

```
        k_total = k_base * parallel_amount / series_amount; % N/mm

    % Length/Deformation
        % Total length of springs in series before deforming
        length_0_total = length_0 * series_amount; % mm

        % Create matrix from max length to undeformed length
        deformation_1 = linspace(deformation_1_max , 0 , rows)'; % mm

        % Length of individual spring
        length_1 = length_0 + deformation_1 ; % mm

        % Maximum length of individual spring
        length_1_max = length_1(1) ; % mm

        % Total deformation for all springs in series
        deformation_total = deformation_1 * series_amount ; % mm

        % Total length for all springs in series
        length_total = length_0_total + deformation_1 * series_amount ; % mm

        % For reference, the maximum total length of all springs in series
        length_total_max = length_0_total + deformation_total ; % mm

        % Arc length the main drum moves each step
        arc_step = [ diff(deformation_total) ; diff(deformation_total(1:2))] ./ 1000 .* -1 .* concentric_ratio; % mm
            % Uniform value assumes linear spring
            % Multiply by concentric pulley ratio as a larger drum has a
            % longer arc length per degree
            % Removes a row. Add one back at the end for future operations

    % Force
        % Total preload for multiple springs
        preload_total = preload * parallel_amount; % N

        % Preload + force from deformation
        force_total = preload_total + deformation_total * k_total ; % N

        % Force that reaches drum after concentric pulleys
        force_effective = force_total / concentric_ratio; % N
            % Because torques are equal, larger radius = lower force

    % Radius
        % Radius of main drum at each step
        radius = torque_target ./ force_effective; % m

        % The radius above in mm
        radius_mm = radius * 1000; % mm

    % Angle
        % Angular displacement of the drum for each step
        angle_drum = arc_step ./ radius; % radians

        % Angular displacement of the armrest for each step
        angle_arm = angle_drum ./ reduction_ratio; % radians
```

```
            % Divide by belt drive ratio as the larger pulley rotates
            % slower than the smaller one

        % Cumulative angular displacement of the armrest, in degrees
        angle_arm_cumulative = cumsum(angle_arm) * 180 / pi; % degrees
            % Must be at least 145

    % Coordinates
        % Angle in radians of each step
        angle_calc = cumsum(angle_drum(calc_start+1:end-calc_end)); % radians

        % Total angle range at armrest
        angle_total = ( angle_calc(end) - angle_calc(1) ) * 180 / pi ./ reduction_ratio; % degrees
            % Must be at least 145

        % Radius of each step in mm
        radius_calc = radius_mm(calc_start+1:end-calc_end); % mm

        % For reference, the angle and radius of each step
        ref_angle_radius = [ angle_calc * 180 / pi , radius_calc ];

        % X coordinate for each step
        x_coord = radius_calc .* cos(angle_calc); % mm

        % Y coordinate for each step
        y_coord = radius_calc .* sin(angle_calc); % mm

        % X and Y coordinates concatenated
        xy_coord = [ x_coord , y_coord ] ; % mm

% Export for spline
    % Add a command to make a spline from coordinates in AutoCAD
    spline = [ "_SPLINE" , "" ; xy_coord ];

    % Export spline script for AutoCAD
    writematrix(spline,"drumspline.csv")
        % Delete comma after _SPLINE
        % Change extension form .csv to .scr
        % Use SCRIPT command

% For reference
angle_arm_ref = angle_arm_cumulative(calc_start+1:end-calc_end) - angle_arm_cumulative(calc_start+1); % degrees
angle_drum_ref = ( angle_calc - angle_calc(1) ) * 180 / pi; % degrees
radius_ref = radius_calc; % mm
deformation_ref = deformation_total(calc_start+1:end-calc_end); % mm
length_ref = length_total(calc_start+1:end-calc_end); % mm
force_spring_ref = force_total(calc_start+1:end-calc_end); % N
force_drum_ref = force_effective(calc_start+1:end-calc_end); % N

final_ref = [ "Arm angle" , "Drum angle" , "Radius" , "Deformation" , "Total Length" , "Force from spring" , "Force at drum" ;
angle_arm_ref , angle_drum_ref , radius_ref , deformation_ref , length_ref , force_spring_ref , force_drum_ref ] ;
```

APPENDIX D
MATLAB CODE FOR SIMULINK MODEL VALUES CALCULATIONS

```
% Constants
    % Range of motion
    range_full = 145 ; % degrees
        % Where 145 degrees is a fully extended (180 degrees) elbow
        % And 0 is a fully flexed (35 degree) elbow

    % Simulation range of motion
    range_sim = 90 ; % degrees

    % Final elbow angle
        % In 180 degree frame of reference
        angle_final = 165 ; % degrees

        % In range of motion frame of reference
        angle_final_rom = range_full - (180 - angle_final) ; % degrees

    % Initial elbow angle
    angle_initial = angle_final_rom - range_sim  ; % degrees

    % Maximum arm reaction torque
    torque_arm_max = 50 ; % Nms

    % Sampling rate
    sampling = 1000 ;

    % Moments of inertia
        % Device
            % Shaft and all components directly attached to it
            i_device_main = 0.04841 ; % kg*m^2

            % Individual pulleys
            i_pulley = 0.00003355 ; % kg*m^2

            i_device = i_device_main + 2 * i_pulley ; % kg*m^2

        % Arm
            % Estimate calculated by simplifying to a long rod
                % 5th percentile female
                mass_arm_f = 1.05 ; % kg
                length_arm_f = 0.294 ; % m
                i_arm_f = mass_arm_f * length_arm_f^2 / 3 ; % kg*m^2

                % 95th percentile male
                mass_arm_m = 2.6; % kg
                length_arm_m = 0.395; % m
                i_arm_m = mass_arm_m * length_arm_m^2 / 3 ; % kg*m^2

    % Efficiency
    efficiency_pulley_1 = 0.98 ;
    efficiency_pulley_2 = 0.98 ;
    efficiency_bearing_1 = 0.99 ;
    efficiency_bearing_2 = 0.99 ;
    efficiency_total = efficiency_pulley_1 * efficiency_pulley_2 *
efficiency_bearing_1 * efficiency_bearing_2 ;

    % Acceleration
```

```
        % Best case scenario acceleration
        acc_max_rad = torque_target * efficiency_total / i_device ; % radians/s^2

        % Coverting to degrees
        acc_max = acc_max_rad * 180 / pi ; % degrees/s^2

        % Worst case scenario acceleration
        acc_min_rad = ( ( torque_target * efficiency_total ) - torque_arm_max ) / ( i_device + i_arm_m ) ; % radians/s^2

        % Coverting to degrees
        acc_min = acc_min_rad * 180 / pi ; % degrees/s^2

% Simulation scenarios
    % Arm reaction torque
            % No arm present
            at0_torque_arm = 0 ; % Nm

            % Torque increasing from 0 to max over range of motion
                % Arm reaction torque as a function of arm angle
                gain_torque_arm_atd = torque_arm_max / range_sim ;

    % Target velocity profile
        % Profile 1
            % Target angular velocity
            vp1_velocity = 100 ; % degrees/s

            % Acceleration
            vp1_acceleration = vp1_velocity * 10 ; % degrees/s^2

            % Ramp time
            vp1_ramp_t = vp1_velocity / vp1_acceleration ; % s

            % Ramp angular displacement
            vp1_ramp_s = vp1_acceleration * vp1_ramp_t^2 / 2 ; % degrees

            % Constant velocity hold duration
            vp1_hold_t = ( range_sim - 2 * vp1_ramp_s ) / vp1_velocity ; % s

            % Total duration
            vp1_duration = 2 * vp1_ramp_t + vp1_hold_t ; % s

            % Linspace range
            vp1_linspace = linspace(0 , vp1_duration , (vp1_duration * sampling)) ;

        % Profile 2
            % Target angular velocity
            vp2_velocity = 6 ; % degrees/s

            % Acceleration
            vp2_acceleration = vp2_velocity * 10 ; % degrees/s^2

            % Ramp time
            vp2_ramp_t = vp2_velocity / vp2_acceleration ; % s

            % Ramp angular displacement
```

```
        vp2_ramp_s = vp2_acceleration * vp2_ramp_t^2 / 2 ; % degrees

        % Constant velocity hold duration
        vp2_hold_t = ( range_sim - 2 * vp2_ramp_s ) / vp2_velocity ; % s

        % Total duration
        vp2_duration = 2 * vp2_ramp_t + vp2_hold_t ; % s

        % Linspace range
        vp2_linspace = linspace(0 , vp2_duration , (vp2_duration * sampling)) ;

    % Profile 3
        % Target angular velocity
        vp3_velocity = 150 ; % degrees/s

        % Acceleration
        vp3_acceleration = vp3_velocity * 10 ; % degrees/s^2

        % Ramp time
        vp3_ramp_t = vp3_velocity / vp3_acceleration ; % s

        % Ramp angular displacement
        vp3_ramp_s = vp3_acceleration * vp3_ramp_t^2 / 2 ; % degrees

        % Constant velocity hold duration
        vp3_hold_t = ( range_sim - 2 * vp3_ramp_s ) / vp3_velocity ; % s

        % Total duration
        vp3_duration = 2 * vp3_ramp_t + vp3_hold_t ; % s

        % Linspace range
        vp3_linspace = linspace(0 , vp3_duration , (vp3_duration * sampling)) ;
```

APPENDIX E
FULL SIMULINK MODEL

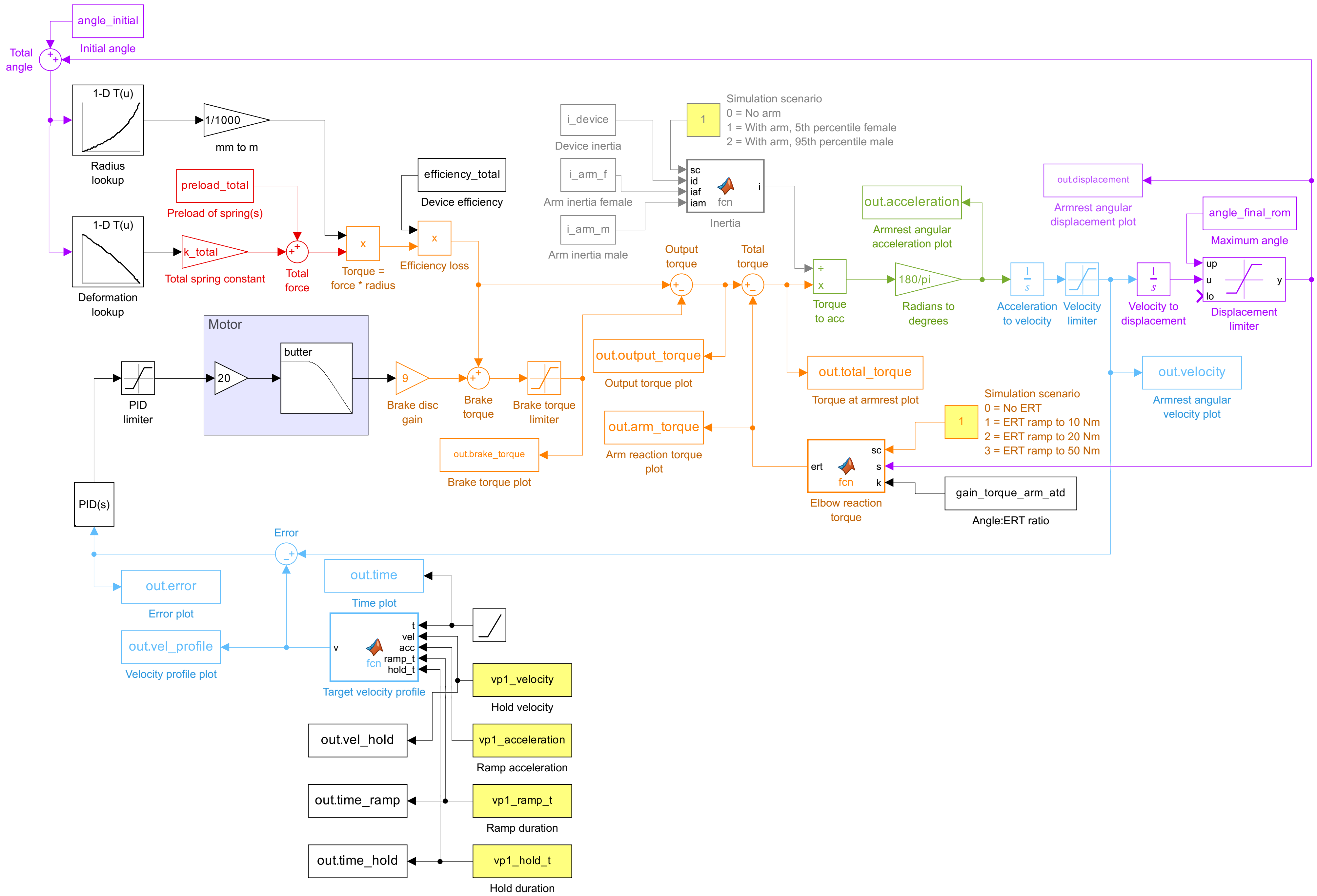

angle_initial
Initial angle
Total angle
1-D T(u)
Radius lookup
1/1000
mm to m
preload_total
Preload of spring(s)
efficiency_total
Device efficiency
1-D T(u)
Deformation lookup
k_total
Total spring constant
Total force
x
Torque = force * radius
x
Efficiency loss
i_device
Device inertia
i_arm_f
Arm inertia female
i_arm_m
Arm inertia male
1
Simulation scenario
0 = No arm
1 = With arm, 5th percentile female
2 = With arm, 95th percentile male
sc
id
iaf
iam
fcn
i
Inertia
out.displacement
Armrest angular displacement plot
out.acceleration
Armrest angular acceleration plot
angle_final_rom
Maximum angle
Output torque
Total torque
Torque to acc
180/pi
Radians to degrees
Acceleration to velocity
Velocity limiter
Velocity to displacement
up
u
lo
y
Displacement limiter
Motor
20
butter
PID limiter
9
Brake disc gain
Brake torque
Brake torque limiter
out.output_torque
Output torque plot
out.total_torque
Torque at armrest plot
out.velocity
Armrest angular velocity plot
Simulation scenario
0 = No ERT
1 = ERT ramp to 10 Nm
2 = ERT ramp to 20 Nm
3 = ERT ramp to 50 Nm
1
out.arm_torque
Arm reaction torque plot
out.brake_torque
Brake torque plot
ert
sc
s
k
fcn
Elbow reaction torque
gain_torque_arm_atd
Angle:ERT ratio
PID(s)
Error
out.error
Error plot
out.time
Time plot
out.vel_profile
Velocity profile plot
v
t
vel
acc
ramp_t
hold_t
fcn
Target velocity profile
vp1_velocity
Hold velocity
out.vel_hold
vp1_acceleration
Ramp acceleration
out.time_ramp
vp1_ramp_t
Ramp duration
out.time_hold
vp1_hold_t
Hold duration

APPENDIX F
MATLAB CODE FOR EVALUATION OF SIMULINK MODEL

```
% Limit arrays to perturbation period
    % Start time
    time_start = 0.1 ;

        % To rows
        eval_start = time_start * 1000 ;

    % End time
    time_end = time_start + out.time_ramp(1) * 2 + out.time_hold(1) ;

        % To rows
        eval_end = time_end * 1000 ;

    % Time array
    eval_time = out.time(eval_start:eval_end) ;

    % Velocity profile array
    eval_vel_profile = out.vel_profile(eval_start:eval_end) ;

    % Velocity output array
    eval_velocity = out.velocity(eval_start:eval_end) ;

    % Error array
    eval_error = out.error(eval_start:eval_end) ;

% Root mean square error
eval_rmse = rmse(eval_vel_profile , eval_velocity) ;

% Maximum error
eval_peak_error = max(abs(eval_error)) ;

% Mean absolute error
eval_mae = mean(abs(eval_error)) ;

% Settling time
    % Limit settling time array so it ends while in steady-state
    st_velocity = eval_velocity(1:end-(out.time_ramp(1) * 1000 + 5)) ;

    % Steady-state velocity
    velocity_ss = st_velocity(end) ;

    % Tolerance
    tolerance = 0.02 ;

    % Upper bound
    st_upper = velocity_ss * (1 + tolerance) ;

    % Lower bound
    st_lower = velocity_ss * (1 - tolerance) ;

    % Find indices where velocity is within bounds
    st_outside_bounds = find(st_velocity < st_lower | st_velocity > st_upper) ;

    % Settling time = last time it goes out of bounds
    eval_settling_time = eval_time(st_outside_bounds(end)) ;
```

```
% Overview
evaluation_overview = [
    "Peak error" , "" , "RMSE" , "" , "MAE" , "" , "SSE" , "" , "Settling time" , "" ;
    "Value" , "Percentage" , "Value" , "Percentage" , "Value" , "Percentage" , "Value" , "Percentage" , "Value" , "Percentage" ;
    eval_peak_error , eval_peak_error / out.vel_hold(1) * 100 , eval_rmse , eval_rmse / out.vel_hold(1) * 100 , eval_mae , eval_mae  / out.vel_hold(1) * 100 , abs(out.vel_hold(1) - velocity_ss) , abs(out.vel_hold(1) - velocity_ss) / out.vel_hold(1) * 100 , eval_settling_time , eval_settling_time / eval_time(end) * 100 ;
    ] ;
```

APPENDIX G
TABLE OF RESULTS FOR ALL SIMULATION SCENARIOS

Target hold velocity/ deg/s	Moment of inertia sources	Max ERT/ Nm	Peak error		RMSE		MAE		SSE		Settling time	
			Value/ deg/s	% of target hold velocity	Value/ deg/s	% of target hold velocity	Value/ deg/s	% of target hold velocity	Value/ deg/s	% of target hold velocity	Value/ s	Percentage of total time
6	PSEP	0	304.49	5074.76	202.80	3380.01	177.42	2956.94	N/A	N/A	N/A	N/A
		10	304.81	5080.17	190.24	3170.72	166.50	2775.04	N/A	N/A	N/A	N/A
		20	305.22	5086.97	172.30	2871.65	149.85	2497.42	N/A	N/A	N/A	N/A
		50	306.51	5108.52	125.56	2092.71	98.37	1639.44	N/A	N/A	N/A	N/A
	PSEP + forearm (F)	0	0.35	5.80	0.02	0.27	0.00	0.03	0.00	0.00	0.24	1.55
		10	0.35	5.80	0.04	0.66	0.04	0.63	0.04	0.61	0.24	1.55
		20	0.35	5.80	0.07	1.24	0.07	1.22	0.07	1.22	0.24	1.55
		50	0.35	5.80	0.18	2.99	0.18	2.98	0.18	2.99	0.24	1.55
	PSEP + forearm (M)	0	0.52	8.62	0.03	0.48	0.00	0.04	0.00	0.00	0.23	1.51
		10	0.52	8.62	0.05	0.76	0.04	0.64	0.04	0.61	0.23	1.51
		20	0.52	8.62	0.08	1.28	0.07	1.24	0.07	1.22	0.23	1.51
		50	0.52	8.62	0.18	3.00	0.18	2.99	0.18	2.99	0.23	1.51
100	PSEP	0	305.89	305.89	175.68	175.68	138.98	138.98	N/A	N/A	N/A	N/A
		10	296.11	296.11	161.59	161.59	128.40	128.40	N/A	N/A	N/A	N/A
		20	283.71	283.71	141.65	141.65	112.80	112.80	N/A	N/A	N/A	N/A
		50	241.96	241.96	89.01	89.01	65.54	65.54	N/A	N/A	N/A	N/A
	PSEP + forearm (F)	0	5.80	5.80	1.04	1.04	0.41	0.41	0.00	0.00	0.24	21.47
		10	5.80	5.80	1.12	1.12	0.82	0.82	0.62	0.62	0.24	21.47
		20	5.80	5.80	1.43	1.43	1.27	1.27	1.22	1.22	0.24	21.47
		50	5.80	5.80	2.85	2.85	2.72	2.72	3.01	3.01	0.24	21.47
	PSEP + forearm (M)	0	8.62	8.62	1.87	1.87	0.55	0.55	0.00	0.00	0.23	20.93
		10	8.62	8.62	1.84	1.84	1.01	1.01	0.62	0.62	0.23	20.93
		20	8.62	8.62	1.98	1.98	1.48	1.48	1.22	1.22	0.23	20.93
		50	8.62	8.62	3.05	3.05	2.88	2.88	3.01	3.01	0.23	20.93
150	PSEP	0	307.10	204.73	165.41	110.27	126.72	84.48	N/A	N/A	N/A	N/A
		10	293.91	195.94	151.90	101.27	117.38	78.26	N/A	N/A	N/A	N/A
		20	272.01	181.34	132.00	88.00	102.77	68.51	N/A	N/A	N/A	N/A
		50	218.99	145.99	78.70	52.47	57.70	38.47	N/A	N/A	N/A	N/A
	PSEP + forearm (F)	0	8.70	5.80	1.87	1.25	0.87	0.58	0.00	0.00	0.24	29.54
		10	8.70	5.80	1.91	1.27	1.35	0.90	0.93	0.62	0.24	29.54
		20	8.70	5.80	2.27	1.51	1.94	1.30	1.84	1.23	0.24	29.54
		50	8.71	5.80	4.16	2.77	3.90	2.60	4.52	3.01	0.24	29.54
	PSEP + forearm (M)	0	12.93	8.62	3.35	2.23	1.18	0.79	0.00	0.00	0.23	28.79
		10	12.93	8.62	3.24	2.16	1.77	1.18	0.93	0.62	0.23	28.79
		20	12.93	8.62	3.35	2.23	2.38	1.58	1.84	1.23	0.23	28.79
		50	12.93	8.62	4.59	3.06	4.24	2.83	4.52	3.01	0.23	28.79